공학박사학위논문

스티어 바이 와이어 시스템의 목표 조향감 재현을 위한 조향 반력 제어

Robust Steering-Assist Torque Control of Steer-by-Wire Systems for Target Steering Wheel Torque Tracking

2020년 2월

서울대학교 대학원

기계항공공학부

이 동 필

Abstract

Robust Steering-Assist Torque Control of Steer-by-Wire Systems for Target Steering Wheel Torque Tracking

Dongpil Lee

School of Mechanical and Aerospace Engineering

The Graduate School

Seoul National University

This dissertation focused on the development of and steering assist torque control algorithm of Electric-Power-Steering (EPS) system from the conventional steering system perspective and Steer-by-Wire (SBW) system. The steering assist torque control algorithm has been developed to overcome the major disadvantage of the conventional method of time-consuming tuning to achieve the desired steering feel. A reference steering wheel torque map was designed by post-processing data obtained from target performance vehicle tests with a highly-rated steering feel for both sinusoidal and transition steering inputs. Adaptive sliding-mode control was adopted to ensure robustness against uncertainty in the steering system, and the equivalent moment of inertia damping coefficient and effective compliance were adapted to improve tracking

performance. Effective compliance played a role in compensating the error between the nominal rack force and the actual rack force. For the SBW system, the previously proposed EPS assist torque algorithm has been also enhanced using impedance model and applied to steering feedback system. Stable execution and how to give the person the proper steering feedback torque of contact tasks by steering wheel system interaction with human has been identified as one of the major challenges in SBW system. Thus, the problem was solved by utilizing the target steering torque map proposed above. The impedance control consists of impedance model (Reference model with the target steering wheel torque map) and controller (Adaptive sliding mode control).

The performance of the proposed controller was evaluated by conducting computer simulations and a hardware-in-the-loop simulation (HILS) under various steering conditions. Optimal steering wheel torque tracking performances were successfully achieved by the proposed EPS and SBW control algorithm.

Keywords: Electric-power-steering system, Steer-by-wire, Vehicle chassis control, Automated driving vehicle, Hardware-in-the-loop simulations

Student Number: 2014-21839

List of Figures

Contents

Chapter 1 Introduction

1.1. Background and Motivation

The steering system translates the driver's steering command into a change of the vehicle's direction. At the same time, the system provides an adequate feedback in order to support the stability of the driver. Since the first steering system form was designed by Alfred Vancheron in 1894 (Eckstein, Hesse, Lutz, & Klein, 2014), numerous steering systems via power-assisted has been invented for driver assistance and vehicle stability with no significant mechanical linkages changes. The design of the power steering system remains functional, but its way of operation has been improved by, for example, introducing hydraulic power-assisted steering (HPS), electrohydraulic power-assisted steering (EHPS), electric power steering (EPS), superimposed steering also known as active front steering (AFS), and steer-by-wire systems (SBW).

Chrysler Corporation introduced the first series production of HPS systems on the 1951 Chrysler Imperial under the name 'Hydraguide'. The principle itself had already been filed in a patent by F.W. Davis in 1926. At first, the system was not used for commercial purposes because it was too expensive, and it was mounted on US military and British military vehicles during World War II. In the HPS system, the pump is driven by the engine of the vehicle. In

recent years, the automotive developers have been focused on energy-efficient steering systems. The researchers have been studied to overcome the inefficiency of the HPS system, which is always running through the belt of the engine. As a result, in the 1990s, EHPS systems have been introduced in which the pump is operated by using an electric motor. Following HPS, and EHPS systems, EPS systems have been presented. The first vehicle having an EPS system was the Suzuki "Cervo" in 1988. This system developed by Koyo (current JTEKT) has an electric motor as a component integrated in the steering column (Nakayama & Suda, 1994). This system allows varying amounts of assistance to be applied depending on driving conditions. Engineers can, therefore, tailor steering-gear response to optimizing ride, handing, and steering for each vehicle (Keebler & Jack, 1986). However, it is time-consuming tuning to achieve a desired steering feel. The next steering design is superimposed steering system also known as active steering, which has been patented in 1974 (U.S. Patent No. 3,831,701, 1974). In 2004, the BMW active steering system allows driver independent steering intervention at the front axle with the mechanical link between the steering wheel and the front axle still in place (Koehn, Philip, & Eckrich., 2004). The system is comprised of a rack-and-pinion steering system, a double planetary gear and an electric actuator motor. This principle enables additional functionality such as a variable steering ratio and improves driving stability. The next generation steering system is steer-by-wire system, which does not have mechanical link between steering wheel and

rack. The steer-by-wire system has been inspired by the fly-by-wire system that has already been used in the aviation industry, and there has been an effort to introduce the system to vehicles. The first reason for the introduction was safety. Before invention of airbag, the steering column often caused severe injuries and many deaths. General Motors presented a research vehicle based on a door-integrated joystick to control the longitudinal and lateral vehicle dynamics in 1962 (U.S. Patent No. 3,022,850, 1962). Steer-by-wire technology is relatively easy to create the desired steering feel compared to conventional systems, because there is no feedback from the road wheel. Currently, since automated driving has been widely considered as a mainstream of the automakers for safety and comfortability, numerous research prototypes and concept cars with steer-by-wire systems have been built and the only most recent example is mentioned in this chapter. In 2017, Nexteer automotive presented Nexteer's steering on demand system, which enables safe natural transitions between manual and automated driving for vehicles capable of SAE Level3, Level 4, and Level 5 automated driving. The system has a Quiet wheel mode function with no steering wheel motion for autonomous mode.

Therefore, this dissertation describes a steering feel generation control algorithm which enhance time-efficiency and steering feel with electric-power-assisted-steering system as well as steer-by-wire system.

1.2. Previous Researches

Over the past decade, steering torque feedback and steering feel performance have been vigorously researched to improve on-center handling, and quantification of vehicle steering feel and responsiveness. Bertollini et al. (Bertollini, P., & Hogan, 1999.)showed that drivers' preferences for steering wheel feel change with vehicle speed, and Green demonstrated that a steering effort that changes with vehicle speed is preferred by driver (Green, Gillespie, Reifeis, L., & Ottens, 1984). Several techniques have been proposed to determine steering feel according to the hysteresis curve (Norman & D, 1984). In addition, numerous studies have attempted to combine subjective and objective criteria. The correlation of subjective and objective methods has been investigated to identify physical parameters that are associated with each other (Farrer & G, 1993). Recently, Jang et al. (Jang, et al., 2014) presented a correlation of subjective and objective measures of on-center handling performance of a vehicle by utilizing an interaction formula obtained from a statistical model that relates driver ratings and key physical parameters. This paper presented the three most influential, large parameters with a statistical correlation through a steering torque and lateral acceleration curve. In this case, the absolute value of the steering torque is defined by the 'looseness' at 0 g of lateral acceleration. In addition, the torque gradient at that part is the 'steering

stiffness', and the instantaneous minimum rate in the range of 0.1 g of lateral acceleration is defined by the 'sharpness on center.' More recently, a study was also performed about the factors that strongly affect steering torque feedback (Jiang, et al., 2015). Despite the substantial amount of extant research on measuring factors that affect steering feel, time-consuming tuning tasks are still required to be applied to real vehicles to utilize these findings. Therefore, developing a common electric-power-steering (EPS) system presents challenges in implementing the steering feel that the developer desires.

Oh et al. (Oh, Chae, Yun, & Han, 2004) described the design of a controller for a steer-by-wire system using a reference torque map. The reference torque map utilized the steering wheel angle and vehicle speed information. Kim et al. (Kim & Song, 2002) presented a control logic with PID control, which comprises a return and active damping function to reduce steering torque effort for an EPS system. In this research, improvement of return-to-center performance was proposed employing a reference steering map defined from vehicle speed and steering wheel angle. Oh et al. and Kim et al. (Oh, Chae, Yun, & Han, 2004) (Kim & Song, 2002) proposed a reference torque map to implement or improve steering wheel torque. However, it is difficult to consider the damping or friction component because the steering angular velocity is not considered in the map. Actually, the steering wheel torque feel possesses a hysteresis affected by friction and damping components. Kim et al. (Kim & Song, 2002) additionally considered active damping control to avoid oscillation

of steering wheel angle. However, the active damping control can act as a hindrance in implementing the desired steering wheel torque.

Steer-by-wire systems are the next generation of steering system and has been studied by many researchers. Hai Wang et al. proposed the control algorithm to converge front wheel steering to a hand wheel reference angle (Wang, Kong, Man, Cao, & Shen, 2014). Also, Pradeep Setlur et al. proposed the continuous time-varing tracking controller for target trajectory tracking (Setlur, Wagner, Dawson, & Braganza, 2006). Ryouhei proposed the active steering control via steer-by-wire system to improve vehicle stability (Hayama & Nishizaki, 2000). The lateral motion control algorithm above can provide stability and comfort to the driver. However, it is also important to study not only the lateral motion of the vehicle but also the steering feel.

A steering torque feedback at the steering wheel, known as steering feel, is important to drivers, who obtain road information using the steering torque feedback. Forsyth et al. observed that without steering feedback, drivers lost all sense of direction in tight turns (Forsyth & Maclean, 2006). Malte et al. showed that the steering feel and vehicle-handling properties are closely related (Nybacka, He, Su, Drugge, & Bakker, 2014). Clearly, generating a good steering feel is important for driver comfort and safety.

Unlike conventional steering systems, in a steer-by-wire system, no steering torque feedback is transmitted to the driver, because there are no mechanical linkages between the steering wheel and the front tires. The elimination of the

mechanical linkage worsens the driver's comfort and safety. Therefore, creating an artificial steering torque feedback is essential for a steer-by-wire system.

Various actuators and sensors are used to generate a steering feel. Farzad et al. used magnetorheological fluid to generate steering feel (Ahmadkhanlou, Washington, Bechtel, & Wang, 2006). Another method is to use a motor. Steve et al. proposed the steering feedback motor torque control algorithm, which is to feed the steering torque directly back to the driver (Fankem & Muller, 2014). This algorithm is composed of modules with various functions such as an active damping module and a friction module. Kim et al. proposed the steering reactive torque map to define targeted steering feel (Kim, Jang, Oh, Lee, & Hedrick, 2008). In this research, the proportional-integral-derivative control method is used to control the steering-wheel feedback motor. Also, Balachandrana proposed targeted steering feel by using the dynamics of the steering system instead of the steering reactive torque map (Balachandran & Gerdes, 2015). D.S. Cheon proposed a steering feedback motor torque control algorithm using variable impedance models (Cheon & Nam, 2017). This algorithm estimates the steering-wheel torque using a disturbance observer instead of a torque sensor. However, these algorithms have different performance depending on hardware specifications. The physical characteristics of the steering system change if additional equipment with additional functions such as mechanical end stopper is attached or sensors are replaced.

In the early 1950s, sliding mode control (SMC) was first proposed, and it was successfully implemented to tackle system uncertainties and external disturbances with good robustness (Slotine, E., & Li, 1991), (Vadim, 1977), (DeCarlo, Zak, & Matthews, 1988). In general, an SMC requires an appropriate control law, such that the sliding mode is reached in a finite amount of time. However, no simple SMC, regardless of whether such uncertainty or disturbance is bounded, nor adaptive sliding mode control (ASMC), has been proposed (Huang, Kuo, & Chang, 2008), (Chang & Yan., 2005). Moreover, integral augmented sliding mode control has been introduced to improve the control performance of a system (EkerI., 2006), (Kunnappillil Madhusudhanan, Corno, & Holweg, 2015).

1.3. Thesis Objectives

This dissertation focused on a novel electric power assisted steering (EPS) and steer-by-wire (SBW) assist motor torque control to overcome the conventional time-consuming tuning method for development by introducing a reference steering wheel torque surface defined by steering angle, angular velocity, and vehicle speed. The proposed algorithm offers expandability to implement various steering wheel torque conditions and different vehicle speeds according to the user's preferences through modifying the reference map. An adaptive sliding mode control algorithm was also proposed for robustness against uncertainties of the steering system parameter to adapt external tire forces. Also, a robust control strategy for generating a steering feel was proposed using haptic impedance control of steer-by-wire systems for tracking of target steering feedback torque. The performance of the proposed algorithm has been investigated via computer simulation and hardware-in-the-loop simulation (HILS) to efficiently evaluate real-time performance.

1.4. Thesis Outline

This dissertation is structured as follows: the dynamic models of steering systems are described in Section 2. In Section 3, target steering wheel torque tracking control which consists of target torque map, adaptive sliding mode control, states estimation, and impedance control is derived. Section 4 presents the simulation and test results for the evaluation of the performance of the proposed algorithm. The contribution of this research and introduction of future works are summarized in Section 5.

Chapter 2 Dynamic Model of Steering Systems

2.1. Dynamic model of Hydraulic/Electrohydraulic Power-Assisted Steering Model

As mentioned above, the first power-assisted steering system is a type of hydraulic power-assisted using the pump driven by engine power. Also, in the case of EHPS, the pump can be driven by electric motor. So, EHPS is the same as the HPS system except for pump driver. In this dissertation, we focused on the development of EPS algorithm, but the hydraulic auxiliary steering system was modeled to know the steering feel of the conventional hydraulic system and to understand its characteristics.

Hydraulic / Electrohydraulic Power-assisted steering systems (HPS/EHPS) can be divided into mechanical and hydraulic parts. The mechanical part consists of steering wheel, upper column, lower column, and rack system as shown in Figure 2.1. And, the hydraulic part is an assist part using pump power driven by engine to help a driver to turn the steering wheel. This part is composed of pump, valve unit, chambers, and tank as can be seen in Figure 2.2.

the steering system dynamics are described as follows:

$$J_{sw}\ddot{\theta}_{sw} = T_{sw} - B_{sw}(\dot{\theta}_{sw}) - FR_{sw}(\dot{\theta}_{sw}) - K_{tbar}(\theta_{sw} - \theta_{col}) \tag{2.1}$$

$$J_{eq}\ddot{x}_r = F_{assist} + \frac{1}{R_{rp}} K_{tbar}(\theta_{sw} - \theta_{col}) - \left[B_r + \frac{B_{col}}{R_{rp}^2} \right](\dot{x}_r) - FR_r(\dot{x}_r) - F_r \tag{2.2}$$

Where θ_{sw}, θ_{col}, and x_r stand for the steering wheel angle, column angle and rack position, respectively. T_{sw}, F_{assist}, and F_r are the steering wheel torque, assist force provided by the hydraulic part, and rack force from changes in the road conditions. $J_{\bullet}$, $M_{\bullet}$, $B_{\bullet}$, $FR_{\bullet}$, and $K_{\bullet}$ represent the moment of inertia, mass, damping coefficient, friction and stiffness, respectively. Also, R_{rp} is the gear ratio between rack and the end of steering column.

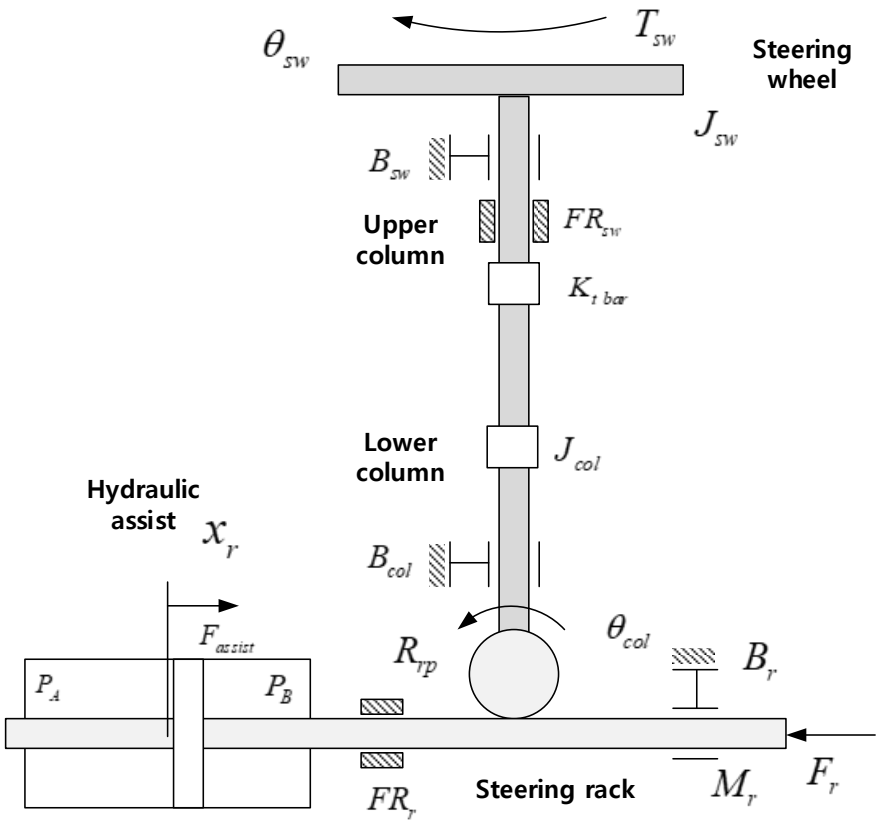

Figure 2.1 Schematic of the mechanical part of HPS/EHPS steering system

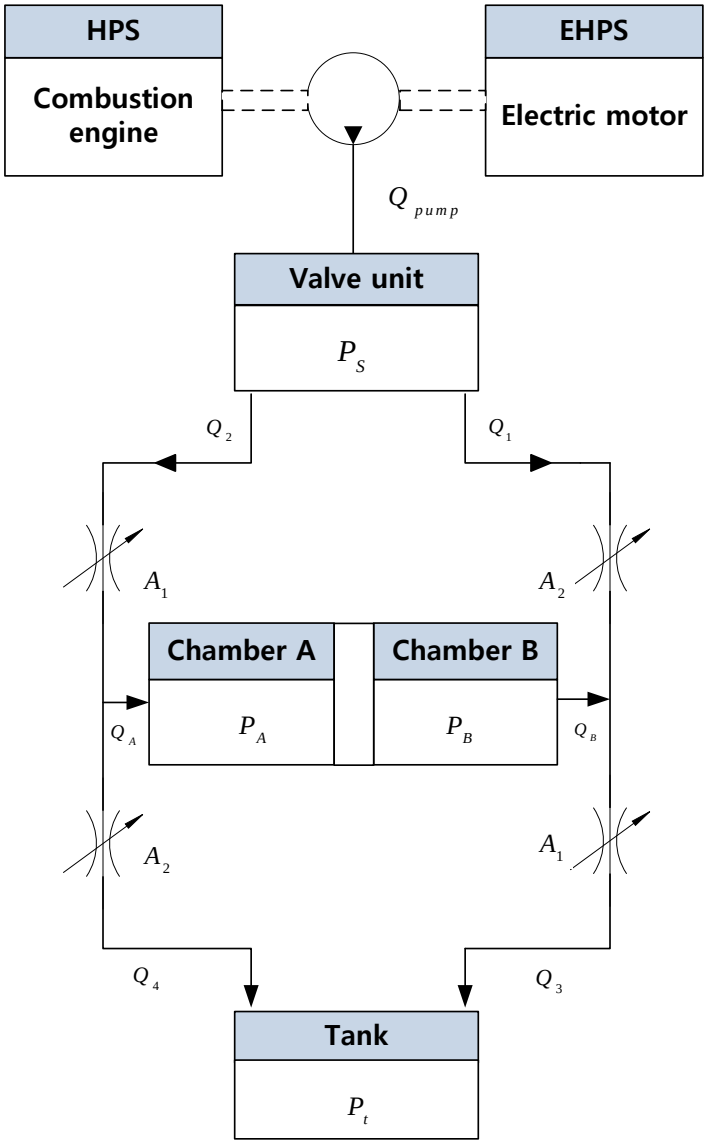

Figure 2.2 Schematic of the hydraulic part of HPS/EHPS steering system

The hydraulic system dynamics are described as follows:

$$
\begin{aligned}
Q_p &= D \cdot \omega \\
Q_1 &= C_d A_1 \sqrt{\frac{2}{\rho}(P_s - P_A)} \\
Q_2 &= C_d A_2 \sqrt{\frac{2}{\rho}(P_s - P_B)} \\
Q_3 &= C_d A_2 \sqrt{\frac{2}{\rho}(P_A - P_t)} \\
Q_4 &= C_d A_1 \sqrt{\frac{2}{\rho}(P_B - P_t)} \\
Q_A &= Q_1 - Q_3 \quad , \quad Q_B = Q_4 - Q_2
\end{aligned}
\tag{2.3}
$$

Where, $Q_{\bullet}$, $P_{\bullet}$, and $A_{\bullet}$ are flow rate, pressure, and valve opening area, respectively. And, C_d denotes discharge coefficient, and ρ denotes density of fluid. The characteristic and angular velocity of pump are D, and ω, respectively. Each equation is to calculate flow rates using the pressure difference. The valve opening area is a mechanical variable valve whose size varies with steering wheel angle position. Also, we can derive the rate of pressure using continuity equation and assist force calculated from chamber pressures as follows:

$$
\begin{aligned}
\dot{P}_s &= \frac{\beta}{V_v}(Q_{pump} - Q_1 - Q_2) \\
\dot{P}_A &= \frac{\beta}{V_{AC} + A_{AC} x_r}(-A_{AC}\dot{x}_r + Q_A) \\
\dot{P}_B &= \frac{\beta}{V_{AC} - A_{AC} x_r}(A_{AC}\dot{x}_r - Q_B)
\end{aligned}
\tag{2.4}
$$

$$F_{assist} = (P_A - P_B)A_{ac} \tag{2.5}$$

Where β denotes bulk modulus. V_v and V_{AC} are value and chamber cylinder volume respectively. Finally, the assist force calculated from (2.5) is applied to the mechanical part.

Figure 2.3 shows a validation results of the simulation model of HPS with actual experiment data. To evaluate the simulation model, weave test was performed with Matlab/Simulink and Trucksim. The experiment data is measured from semi-bonnet vehicle of Hyundai. The simulation result and experiment data were confirmed to be well matched.

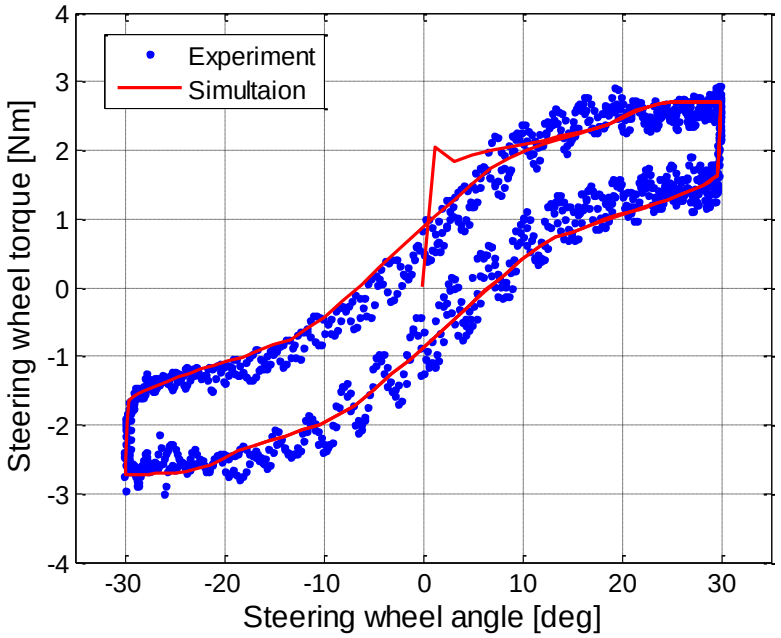

Figure 2.3 Weave test at 30 deg, 80 km/h, 0.2 Hz

2.2. Dynamic model of Electric-Power-Assisted-Steering Model

A column type electric-power-assisted-steering (CEPS) model is utilized to design the steering assist torque control law. CEPS is one of the steering system types that is supported by electric motor power on the column. Zhang et al. presented a mathematical model and characteristic curves of an EPS system (Zhang, Zhang, Liu, Ren, & Gao, 2009). The steering system comprise a steering wheel, upper column, lower column, electric motor, and steering rack, as shown in Figure 2.4, and the steering system dynamics are described as (2.6) ~(2.8) without electric motor dynamics

$$J_{sw}\ddot{\theta}_{sw} + B_{sw}\dot{\theta}_{sw} = T_{sw} - K_{tbar}\left(\theta_{sw} - \frac{x_r}{R_{rp}}\right) \tag{2.6}$$

$$J_m\ddot{\theta}_m + B_m\dot{\theta}_m = T_m - K_m\left(\theta_m - R_G\frac{x_r}{R_{rp}}\right) \tag{2.7}$$

$$M_r\ddot{x}_r + B_r\dot{x}_r + K_r x_r = \frac{R_G K_m}{R_{rp}}\left(\theta_m - R_G\frac{x_r}{R_{rp}}\right) + \frac{K_{tbar}}{R_{rp}}\left(\theta_{sw} - \frac{x_r}{R_{rp}}\right) - F_r \tag{2.8}$$

Where

$$T_m = K_t i_m$$

Where θ_{sw}, θ_m, and x_r stand for the steering wheel angle, motor angle and rack position, respectively. T_{sw}, T_m, and F_r are the steering wheel torque,

assist torque provided by the electric motor, and rack force from changes in the road conditions. $J_{\bullet}$, $M_{\bullet}$, $B_{\bullet}$, and $K_{\bullet}$ represent the moment of inertia, mass, damping coefficient, and stiffness, respectively. Also, R_{rp} is the gear ratio between rack and the end of steering column, and R_G is motor gear ratio between steering column and motor gear. Where K_t is the motor torque constant, and i_m is the current in the electric motor, respectively.

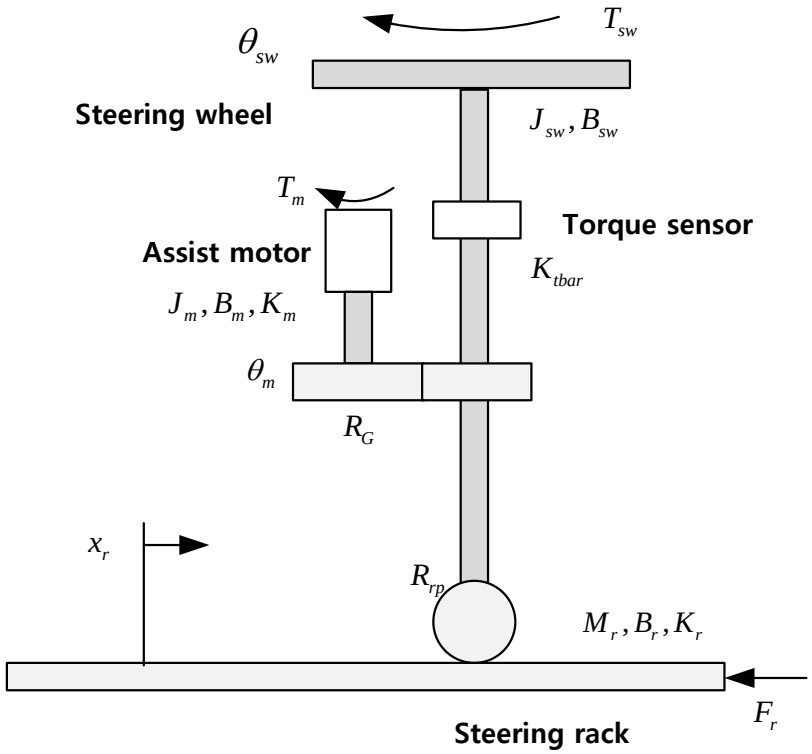

Figure 2.4 Schematic of a column-type electric power assisted steering system

Yih *et al.* (Yih & Gerdes, 2005) represented the dynamics of the steering system utilizing a simple second-order model to modify the vehicle handling characteristics via steer-by-wire. Yih proposed that the frequency response of the system can be approximated by using the empirical transfer function estimate (ETFE), i.e., the ratio between the output and input discrete Fourier transform (DFT). Yih assumed that the transfer function could represent the steering system, including the total moment of inertia, the effective viscous damping coefficient, the Coulomb friction, and the disturbance from the tire force and aligning moment.

Therefore, the simple second-order model is proposed as follows:

$$J_{eq}\ddot{\theta}_{sw} + B_{eq}\dot{\theta}_{sw} = T_{sw} + T_m - K_{eff}\,\theta_{sw} - R_{rp}F_r \tag{2.9}$$

where J_{eq} and B_{eq} are the system equivalent moment of inertia and damping coefficient. T_{sw}, T_m, K_{eff}, and F_r are steering torque, assist torque, effective compliance, and rack force, respectively. R_{rp} is the gear ratio between the rack and the end of the steering column. Most of the disturbance in steering systems is the rack force, F_r, from tire forces. Hence, the rack force information is critical to implement the controller for steering systems. Gillespie (Gillespie, 1992) reported that the steering system could be represented by effective compliance in the low-frequency range. The following

experiments were conducted to identify the characteristics of rack force. Figure 2.5 shows the forces under different vehicle speed and road fiction with weave tests at 0.2 Hz and 60 deg open-loop command using Carsim software E-Class Sedan. As can be seen in Figure 2.5, the rack force increases linearly as the steering wheel angle increases. Also, the rate of the rack force corresponding to the steering wheel angle increase as the vehicle speed increases. As a result, the rack force has linearity until the tire forces are saturated. Therefore, the rack force was assumed to be linear using effective compliance, K_{eff} , and selected as an adaption parameter. Effective compliance plays a role in compensating for the error between the nominal rack force and the actual rack force.

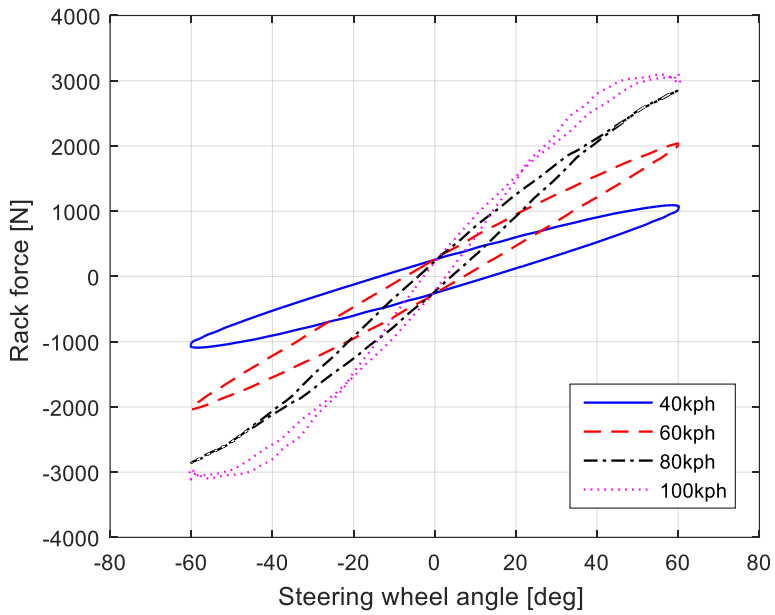

Figure 2.5 Comparison of different vehicle speed : rack force.

2.3. Dynamic model of Steer-by-Wire Model

‘

The steer-by-wire system (SBW) consists of a steering-wheel system, and a rack system. Depending on how the developer design this system, the only difference from conventional steering systems is that there are no columns. And a steering feedback motor and rack actuator part should be added to replace the part. the steering feedback motor generates steering feel while drivers apply steering wheel torque to turn the steering wheel. So, the drivers can feel only the reaction torque from the steering feedback motor without any disturbance from the rack system. The rack actuator should conduct the steer control to track the steering wheel angle which is measured from torque and angle sensor. Therefore, the steer-by-wire system must comprise at least a steering feel generation and a rack actuator algorithm.

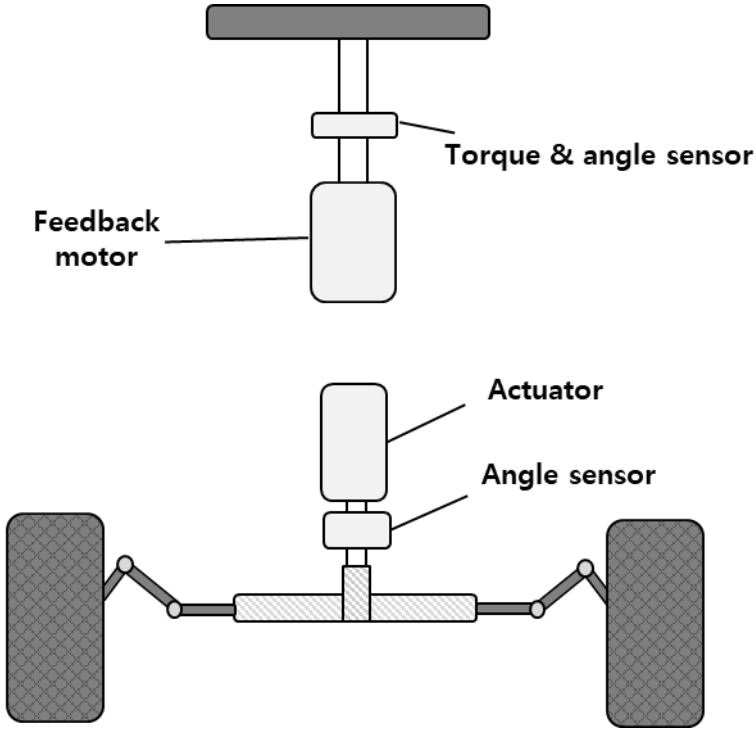

Figure 2.6 Schematic of a steer-by-wire steering system

2.4. Rack force characteristic of steering system

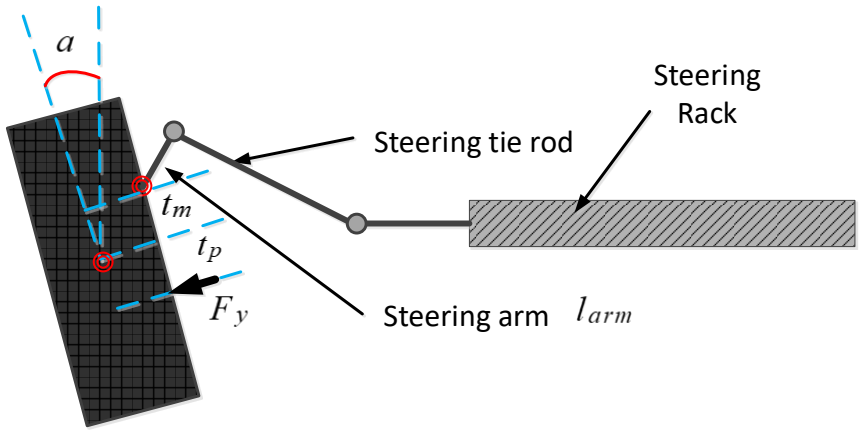

Figure 2.7 Components of steering rack system

The biggest impact in the steering system is the rack force from the tires. Figure 2.7 shows components of steering rack system. Although the various steering systems have been described earlier, this section will cover the details of the rack force. Rack force basically has movements based on elastic kinematics. Strictly, we can calculate the alignment torque by the lateral force from the tire as

$$\begin{aligned} M_{align} &= F_y\left(t_m + t_p\right) \\ t_m &= \Delta + R_{eff}\,\theta \\ t_p &= t_{p0} - \frac{t_{p0}C_\alpha}{3\mu F_z}\left|\tan\alpha\right| \end{aligned} \tag{2.10}$$

where, t_m, mechanical trail is a trail which is calculated by kingpin axis offset, Δ, from center of the tire plus caster angle, θ, multiplied by effective radius

of tire, R_{eff}, and t_{p0}, t_p denote initial pneumatic trail and pneumatic trail which is the distance that the resultant force of side-slip occurs behind the geometric center of the contact patch. The pneumatic trail is related with tire characteristic such as slip-angle, α, cornering stiffness, C_α, friction, μ, and tire normal force, F_z. From (2.10), we can calculate an actual rack force as follows:

$$F_r = \frac{M_{align}}{l_{arm}} \tag{2.11}$$

where, l_{arm} denote steering arm length, and F_r is rack force.

Rack force measurement have been conducted with Genesis G80 using strain gauge on each tie rod as shown in Figure 2.8. In compression, the tie rod force was measured negative value. On the contrary, in tension, it is measured positively. The results of rack force measurement are described in Figure 2.9. The transition test was carried out at 60 km/h. As mentioned above, the left tie rod was measured negatively, and the right tie rod was measured positively. The rack force was calculated from sum of the left and right tie road force (Compression and tensile just represent direction of force). In this way, weave tests according to vehicle speed were conducted to analyze the rack force characteristic as shown in Figure 2.10. The characteristics of rack force can be seen that the gradient increases with vehicle speed as mentioned in section 2.2. The difference from the simulation is that the hysteresis thickness is thick

in the relatively low speed region. These characteristics will be used to design steering feel generation.

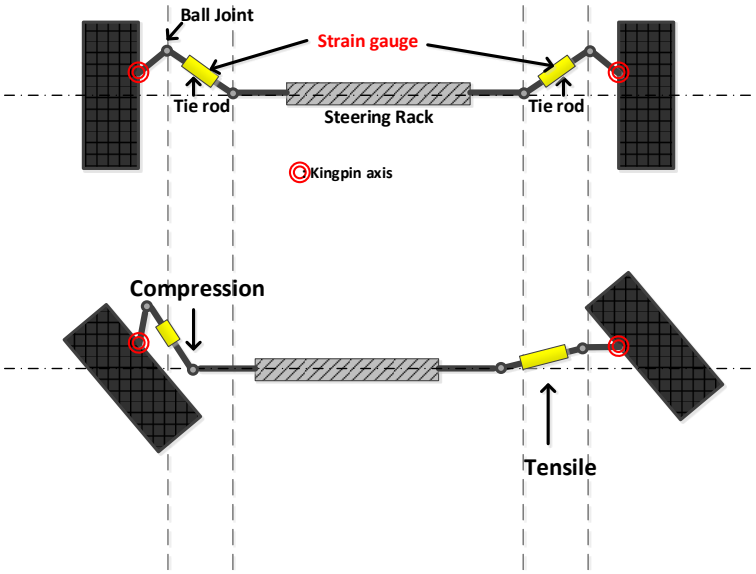

Figure 2.8 Experiment setting for rack force measurement of Genesis G80

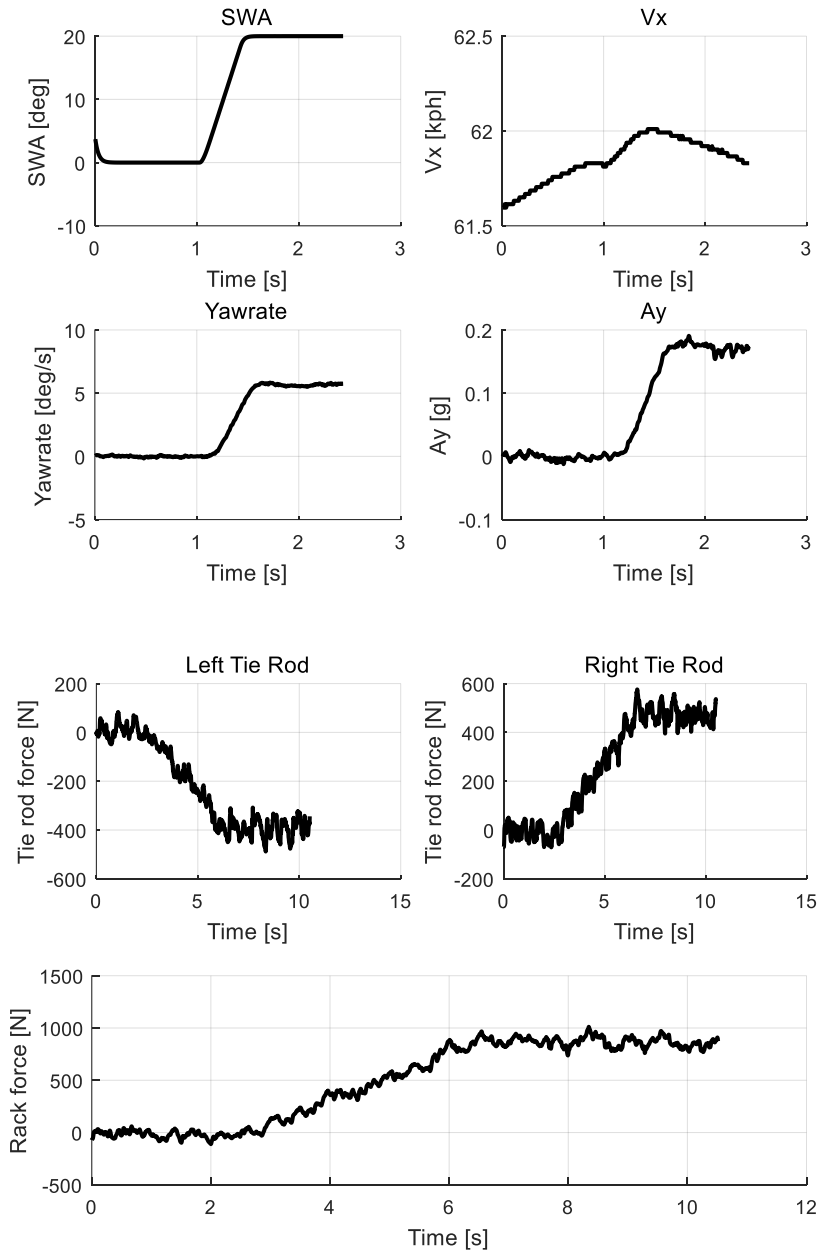

Figure 2.9 Measurement results of rack force with Genesis G80 at 60 km/h

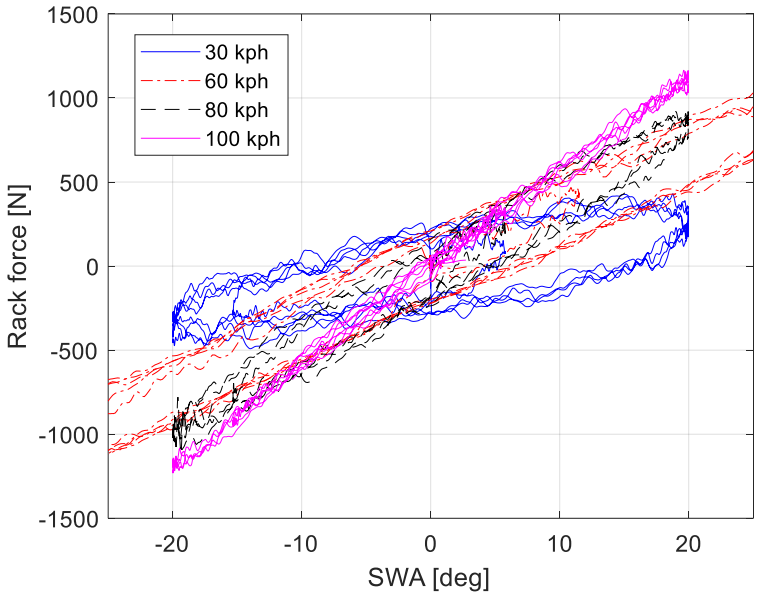

Figure 2.10 Rack force according to vehicle speed

Chapter 3 Target steering wheel torque tracking control

3.1. Target steering torque map generation

The steering characteristics are measured by conducting various tests. Sinusoidal and transition tests constitute typical test scenarios for steering characteristics. The sinusoidal test, which is also known as a weave test, measures the characteristics of the steering system, such as the degree of hysteresis and the assist torque. The transition test is carried out under constant steering angular velocity to measure the initial assist torque through the EPS logic or the characteristics of the vehicle dynamics. These characteristics of tests are utilized to determine the target steering torque map from the steering wheel angle, steering angular velocity and vehicle speed, as shown in Figure 3.1. Therefore, the damping or friction component should be considered when designing a target steering wheel torque. This component also implies that the target steering wheel torque exists, regardless of the steering angle, as long as the steering wheel has velocity. Consequently, the target steering wheel torque is created as a friction model to make a hysteresis to enhance on-center handling. The target steering wheel torque is presented at 40, 60, and 80 km/h. If a

developer desires to alter the speed of the vehicle, multiplication on low-gain at low vehicle speed and high-gain at high vehicle speed could be applied, as Oh et al. (Oh, Chae, Yun, & Han, 2004) proposed. Hence, utilizing the target map will not only achieve the desired steering wheel torque, but will also enhance steering feel, which is highly beneficial for the driver.

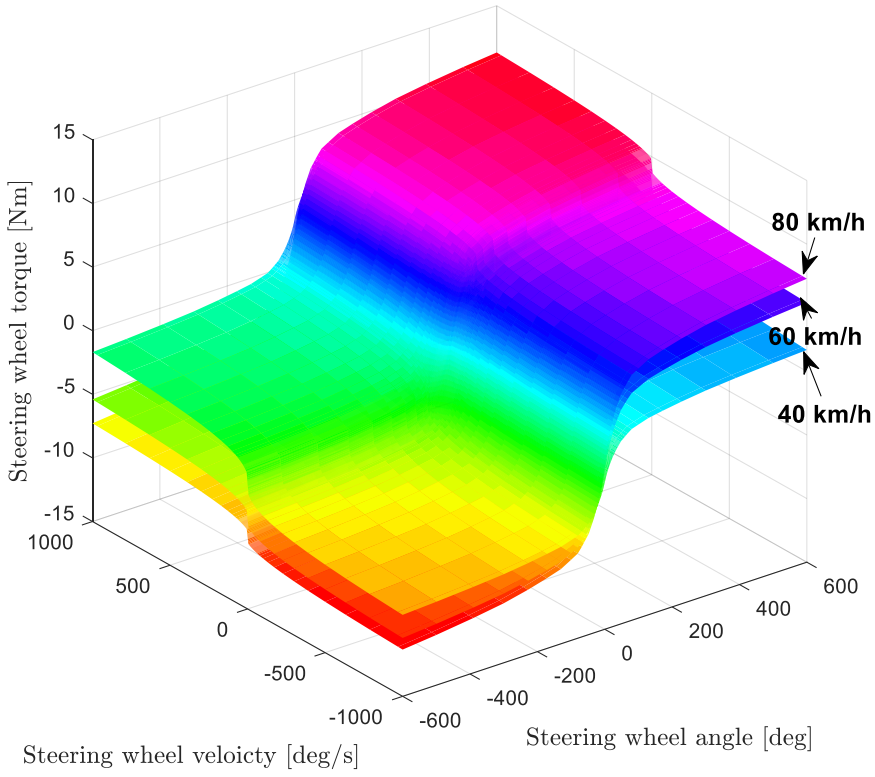

Figure 3.1 Target steering wheel torque surface at 40, 60, and 80 km/h

3.2. Adaptive sliding mode control design for target steering wheel torque tracking with EPS

The electric-power-assisted-steering systems (EPS) algorithm function consists of three parts, as shown in Figure 3.2. The assist torque control uses the sensor information of EPS and vehicle chassis. The target steering wheel torque map is designed by the steering angle, steering angular velocity, and longitudinal velocity of the vehicle. The nominal rack force is calculated using the linear tire model with the vehicle sensor information, and steering states with a Kalman filter are estimated to implement the adaptive sliding mode control (ASMC). Finally, the ASMC controller is used for the target steering wheel torque tracking. The ASMC calculates the assist torque input of the EPS of the steering system at every time-step.

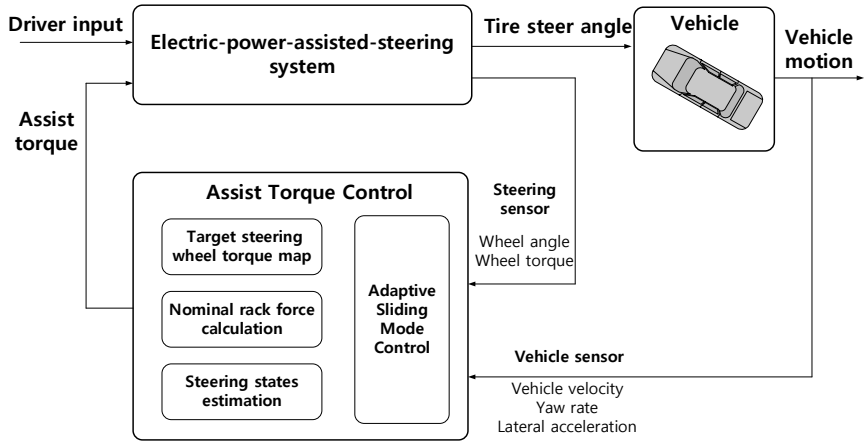

Figure 3.2 EPS control algorithm for the target steering wheel torque tracking.

As mentioned above, the steering dynamics in Eq.(2.9) are used for the control law. However, this model inevitably introduces some approximations and uncertainties, as follows:

$$\left(\hat{J}_{eq}+\Delta J_{eq}\right)\ddot{\theta}_{sw}+\left(\hat{B}_{eq}+\Delta B_{eq}\right)\dot{\theta}_{sw}=T_{sw}+T_m-\left(\hat{K}_{eff}+\Delta K_{eff}\right)\theta_{sw} \\ -R_{rp}\hat{F}_r-\Delta_{un} \tag{3.1}$$

where $\hat{\bullet}$, and $\Delta\bullet$ are the nominal value and uncertainty of the value, respectively; and Δ_{un} is unmodeled term of steering system. To account for uncertainties, the model uncertainties and nonlinearities are assumed to be as shown in Eq. (3.1). This assumption is referred to as the matching condition (DeCarlo, Zak, & Matthews, 1988).

$$\hat{J}_{eq}\ddot{\theta}_{sw} + \hat{B}_{eq}\dot{\theta}_{sw} = T_{sw} + T_m - \hat{K}_{eff}\theta_{sw} - R_{rp}\hat{F}_r + L(t) \tag{3.2}$$

where $L(t)$ denotes the lumped uncertainty that is bounded, but unknown; $|L(t)| \le L_m$; and L_m are positive real constants, $L(t)$ is defined by

$$L(t) = -\Delta J_{eq}\ddot{\theta}_{sw}(t) - \Delta B_{eq}\dot{\theta}_{sw}(t) - \Delta K_{eff}\theta_{sw}(t) - \Delta_{un} \tag{3.3}$$

The sliding surface can be improved by introducing an integral action into the sliding surface for the steady-state accuracy, defined as (EkerI., 2006)

$$e(t) = T_{sw}(t) - T_{sw.des}(t) \tag{3.4}$$

$$s(t) = \lambda_1 e(t) + \lambda_2 \int_0^t e(\tau)\, dt \tag{3.5}$$

where λ_1 and λ_2 are positive gains, and $T_{sw.des}$ is the steering feel torque from the four-dimension map. The appropriate gains are selected to enhance performance. The sliding controller aims to design a control law that efficiently accounts for both parameter uncertainty and the presence of unmodeled dynamics (Slotine, E., & Li, 1991). The sliding control has continuous and discontinuous parts where the continuous part is the equivalent control assuming the lumped vector L in Eq.(3.2) and the discontinuous section compensates for uncertainties and nonlinearities.

The derivative of sliding variable $\dot{s}$ given by

$$\dot{s}(t) = \lambda_1 \dot{e}(t) + \lambda_2 e(t) \tag{3.6}$$

neglecting the parametric uncertainties and the friction and utilizing the nominal parameters in Eq.(3.2). As a result, the equivalent control u_{eq} is obtained as follows:

$$u_{eq} = \hat{J}_{eq}\ddot{\theta}_{sw} + \hat{B}_{eq}\dot{\theta}_{sw} + \hat{K}_{eff}\theta_{sw} + R_{rp}\hat{F}_r - T_{sw.des} + \frac{\lambda_1}{\lambda_2}\dot{e} \tag{3.7}$$

In order to guarantee the robustness of the controller against the parametric uncertainties, a switching control input u_N is introduced as

$$u_N = k\ \mathrm{sat}\left[s(t)/\Phi\right] \tag{3.8}$$

where k refers to the upper bound of the uncertainty, i.e., $|L_m| \le k$; and Φ is a positive constant that defines the thickness of the boundary layer that affects the steady-state accuracy and robustness. Under this condition, the system can be expected to be stable, and $\mathrm{sat}\left[s(t)/\Phi\right]$ denotes the saturation function, defined as

$$\mathrm{sat}\left[s(t)/\Phi\right] = \begin{cases} 1 & if\ s(t) > \Phi \\ -1 & if\ s(t) < -\Phi \\ s(t)/\Phi & else \end{cases} \tag{3.9}$$

Lastly, where $\hat{J}_{eq}$, $\hat{B}_{eq}$, and $\hat{K}_{eff}$ denote the adjusted parameter for compensating uncertainties in Eq.(3.7), whose adaptation laws are given by

$$\dot{\hat{J}}_{eq}(t) = \frac{1}{\rho_J} s(t) \cdot \ddot{\theta}_{sw}(t) \tag{3.10}$$

$$\dot{\hat{B}}_{eq}(t) = \frac{1}{\rho_B} s(t) \cdot \dot{\theta}_{sw}(t) \tag{3.11}$$

$$\dot{\hat{K}}_{eff}(t) = \frac{1}{\rho_K} s(t) \cdot \theta_{sw}(t) \tag{3.12}$$

where ρ_J, ρ_B, and ρ_K, which are positive constants, denote the adaptation gain to be designed. Finally, the total control input u is as follows:

$$u(t) = T_m(t) = u_{eq}(t) + u_N(t) \tag{3.13}$$

with u_{eq} defined in (3.7), and u_N in (3.8) respectively. Then, consider the candidate Lyapunov function $V(t)$ to prove that the tracking error (3.4) of the system can asymptotically converge to zero for a given reference steering wheel angle with total control input u in (3.13). The Lyapunov function is as follows:

$$V(t) = \frac{1}{2} s(t)^2 + \lambda_2 \left[\frac{\rho_J}{2} (\Delta J_{eq})^2 + \frac{\rho_B}{2} (\Delta B_{eq})^2 + \frac{\rho_K}{2} (\Delta K_{eff})^2 \right]$$
$$\left(J_{eq} = \hat{J}_{eq} + \Delta J_{eq},\ B_{eq} = \hat{B}_{eq} + \Delta B_{eq},\ K_{eff} = \hat{K}_{eff} + \Delta K_{eff} \right) \tag{3.14}$$

The derivative of V along the system trajectory is

$$\dot{V}(t) = s \cdot \dot{s} + \lambda_2 \begin{bmatrix} \rho_J \Delta J_{eq} \left(\dot{J}_{eq} - \dot{\hat{J}}_{eq} \right) + \rho_B \Delta B_{eq} \left(\dot{B}_{eq} - \dot{\hat{B}}_{eq} \right) \\ + \rho_K \Delta K_{eff} \left(\dot{K}_{eff} - \dot{\hat{K}}_{eff} \right) \end{bmatrix} \tag{3.15}$$

We assume J_{eq}, B_{eq}, and K_{eff} are constant if vehicle speed is constant. Therefore, we have

$$\begin{aligned} \dot{V}(t) &= s \cdot \dot{s} + \lambda_2 \left[\rho_J \Delta J_{eq} \left(-\dot{\hat{J}}_{eq} \right) + \rho_B \Delta B_{eq} \left(-\dot{\hat{B}}_{eq} \right) + \rho_K \Delta K_{eff} \left(-\dot{\hat{K}}_{eff} \right) \right] \\ &= s \cdot \dot{s} - \lambda_2 \left[\Delta J_{eq} s \cdot \ddot{\theta}_{sw} + \Delta B_{eq} s \cdot \dot{\theta}_{sw} + \Delta K_{eff} s \cdot \theta_{sw} \right] \\ &= s \left[\lambda_1 \dot{e} + \lambda_2 \left(J_{eq} \ddot{\theta}_{sw} + B_{eq} \dot{\theta}_{sw} - T_m + K_{eff} \theta_{sw} + R_{rp} F_r - T_{sw.des} \right) \right] \\ &\quad - \lambda_2 \left[\Delta J_{eq} s \cdot \ddot{\theta}_{sw} + \Delta B_{eq} s \cdot \dot{\theta}_{sw} + \Delta K_{eff} s \cdot \theta_{sw} \right] \end{aligned} \tag{3.16}$$

Substituting the control input (3.13) into (3.16) yields

$$\begin{aligned} \dot{V}\left(s(t)\right) &= s \left\{ \lambda_1 \dot{e} + \lambda_2 \begin{bmatrix} J_{eq} \ddot{\theta}_{sw} + B_{eq} \dot{\theta}_{sw} - T_{sw.des} + K_{eff} \theta_{sw} + R_{rp} \hat{F}_r \\ -\left(u_{eq} + u_N \right) \end{bmatrix} \right\} \\ &\quad - \lambda_2 \left[\Delta J_{eq} s \cdot \ddot{\theta}_{sw} + \Delta B_{eq} s \cdot \dot{\theta}_{sw} + \Delta K_{eff} s \cdot \theta_{sw} \right] \\ &= \lambda_2 \left[\Delta_{un} - k \cdot s(t) \ \mathrm{sat}\left(s(t) / \Phi \right) \right] \end{aligned} \tag{3.17}$$

Since $|\Delta_{un}| < |L_m| \le k$, $\dot{V}$ is strictly negatively defined. Thus, the system with the control input in (3.13) is asymptotically stable.

The aligning moment to calculate the nominal rack force, $\hat{F}_r$, constitutes most of the disturbance in steering systems. There are various ways to calculate the moment. Pacejaka (Pacejka & Besselink, 1997) proposed aligning torque

equations using the magic formula tire model. However, this requires many states of the tire model. On the other hand, Yih et al. (Yih & Gerdes, 2005) proposed a self-aligning torque based on a map with lateral force by multiplying the pneumatic trail as a tire slip angle. Pfeffer et al. (Pfeffer, Harrer, & Johnston, 2008) used a simple equation in which the aligning torque from the lateral tire force is calculated by multiplying the lateral tire force with the mechanical and pneumatic trail. Therefore, the nominal rack force, $\hat{F}_r$, from the aligning torque is just computed using the linear tire model in which the slip angle is assumed to exist in linear areas, and the error between the actual rack force and the model is compensated by implementing the adaption techniques as mentioned above. The nominal rack force is calculated as follows:

$$\hat{F}_r = \frac{2}{L_{arm}} \cdot \left[C_f \left(\delta_{tire} - \frac{V_y + l_f \cdot \gamma}{V_x} \right) \right] (t_m + t_p) \tag{3.18}$$

where L_{arm} is the steering arm length; C_f is the front lateral tire stiffness; δ_{tire} is the front tire angle; V_x and V_y are the longitudinal and lateral velocity of the vehicle, respectively; l_f is the distance between C.G. and the front tire; γ is the yaw rate of vehicle; t_m is the mechanical trail; and t_p is the pneumatic trail. Assuming that the left front tire force and the right front tire force are identical for convenience, t_m and t_p are positive constants. All

vehicle state information, such as the lateral velocity or side slip angle, are very difficult or expensive to measure directly. During the last few years, significant research on estimation of vehicle side slip angle has been conducted (Chen & Hsieh, 353-364), (Bevly, Ryu, & Gerdes, 2006), (Piyabongkarn, Rajamani, Grogg, & Lew, 2009). A side slip angle estimator using global positioning system (GPS) measurements has been proposed (Chen & Hsieh, 353-364). Other methods for estimating the side slip angle based on a kinematic model using the extended Kalman filter (Bevly, Ryu, & Gerdes, 2006) or a combination of kinematic and dynamics model using lateral acceleration and yaw rate motion measurements (Piyabongkarn, Rajamani, Grogg, & Lew, 2009) have been evaluated. It was assumed that the side slip angle of a vehicle can be obtained by a side slip angle state estimator that was designed in previous research. Although this simple rack force from the linear tire model using estimated state or nominal parameter is not accurate compared to actual rack force, the error is compensated through adapting the effective compliance parameter. Therefore, the effective compliance force, $\hat{K}_{eff}\theta_{sw}$, with the nominal rack force, $\hat{F}_r$, approaches the actual rack force. For this paper, the vehicle parameters are shown in Table 1

Table 1 Vehicle parameters

Parameter	Value	Units
l_f	107.95	mm
C_f	24.5	kN
t_m	2.6	cm
t_p	1.4	cm

3.2.1. Steering states estimation with a kalman filter

It is essential to filter signals to improve controller performance, and a Kalman filter and a low-pass filter are utilized in this research. The steering system is equipped with a steering angle, as well as steering wheel torque sensors. Ideally, this signal should be reasonably clean since high-frequency noise tends to worsen with differentiation, and heavy filtering might induce a lag in the signal (Yih & Gerdes, 2005). Therefore, the solution to obtain $\dot{\theta}_{sw}$, $\ddot{\theta}_{sw}$, and T_{sw} is to pass the measured steering wheel angle $\theta_{sw,sensor}$ with the Kalman filter and $T_{sw,sensor}$ through the first-order filter. The Kalman filter state vector, $\mathbf{x}$, and the state space equation are defined as follows:

$$\mathbf{x} = \begin{bmatrix} \theta_{sw} & \dot{\theta}_{sw} & \ddot{\theta}_{sw} \end{bmatrix}^T \tag{3.19}$$

$$\mathbf{x}[k+1] = \mathbf{A}_d \mathbf{x}[k] + \mathbf{w}[k] \tag{3.20}$$

where,

$$\mathbf{A}_d = \begin{bmatrix} 1 & \Delta T & \Delta T^2 / 2 \\ 0 & 1 & \Delta T \\ 0 & 0 & 1 \end{bmatrix}$$

where $\mathbf{w}[k]$ denotes the process noise that is assumed to have been drawn from a zero-mean multivariate normal distribution with covariance $\mathbf{Q}_k$; and ΔT is the sampling time (0.001 s in this study). The state transition model is designed using the kinematics relationship of steering motion. Therefore, since the position-velocity and the velocity- acceleration relationship is correctly a differential relationship, all of the matrix elements are zero, except for the third row and third column value of the covariance $\mathbf{Q}_k$. For this reason, $\mathbf{Q}_k^{3,3} = 100$ is chosen for implementation.

Only the steering angle is assumed to be in a measurable state, and thus the measurement model can be defined as follows:

$$\mathbf{z}[k] = \mathbf{H}\mathbf{x}[k] + \mathbf{v}[k] \tag{3.21}$$

Where,

$$\mathbf{H} = \begin{bmatrix} 1 & 0 & 0 \end{bmatrix}$$

where $\mathbf{v}[k]$ is the observation noise that is assumed to be the zero mean

Gaussian white noise with covariance $\mathbf{R}_k$. As can be seen from the estimation results below in Fig. 5(a), the angle sensor used in the steering system does not possess much noise. Therefore, $\mathbf{R}_k^{1,1} = 0.1$ is chosen for implementation.

The above process model and measurement model are used with the Kalman filter to estimate steering angular velocity and steering angle acceleration. The sequence for the Kalman filter, which recursively estimates the states at each time-step, is composed of time and measurement updates as defined by:

· *Time update*

$$\begin{aligned} \bar{\mathbf{x}}[k] &= \mathbf{A}_d[k] \cdot \hat{\mathbf{x}}[k-1] \\ \bar{\mathbf{P}}[k] &= \mathbf{A}_d[k] \cdot \hat{\mathbf{P}}[k-1] \cdot \mathbf{A}_d{}^T[k] + \mathbf{Q}_k \end{aligned} \tag{3.22}$$

· *Measurement update*

$$\begin{aligned} \mathbf{K}[k] &= \bar{\mathbf{P}}[k] \cdot \mathbf{H}^T \cdot (\mathbf{H} \cdot \bar{\mathbf{P}}[k] \cdot \mathbf{H}^T + \mathbf{R}_k)^{-1} \\ \hat{\mathbf{P}}[k] &= (\mathbf{I} - \mathbf{K}[k] \cdot \mathbf{H}) \cdot \bar{\mathbf{P}}[k] \\ \hat{\mathbf{x}}[k] &= \bar{\mathbf{x}}[k] + \mathbf{K}[k] \cdot (\mathbf{z}[k] - \mathbf{H} \cdot \bar{\mathbf{x}}[k]) \end{aligned} \tag{3.23}$$

where $\mathbf{P}[k]$, $\mathbf{K}[k]$, and $\hat{\mathbf{x}}[k]$ are the error covariance, Kalman gain, and estimated state, respectively, at the k-th time-step. The steering states are estimated well, as shown in Figure 3.3. Figure 3.3 (a) and (d) show the results for the steering wheel angle. As shown in Figure 3.3 (d), the measured steering

wheel angle represents the discretized value from the sensor of the EPS system. Figure 3.3 (b) and (c) represent the steering angular velocity and the angular acceleration from the sensor and the estimation, respectively. The sensor uses a derivative of the measured steering wheel angle and low-pass filter to reduce high-frequency values. Since the discretized values are directly differentiated, the high-frequency components remain as shown in Figure 3.3 (b) and (c). If a low-pass filter is used to reduce the high-frequency values, the desired performance will not be expected due to the phase delay problem. On the other hand, the estimated value indicates that the high-frequency component has been removed.

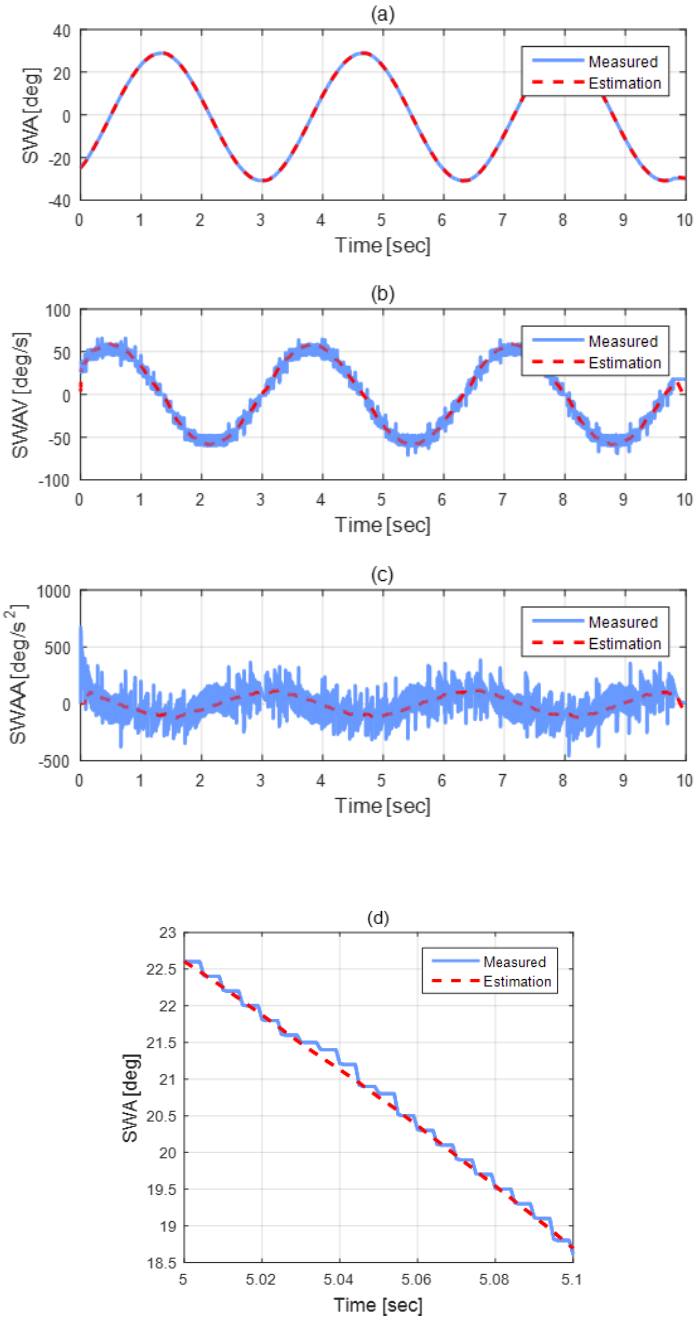

Figure 3.3 Steering states estimation results with hard-ware-in-loop simulation.

3.3. Impedance Control Design for Target Steering Wheel Torque Tracking with SBW

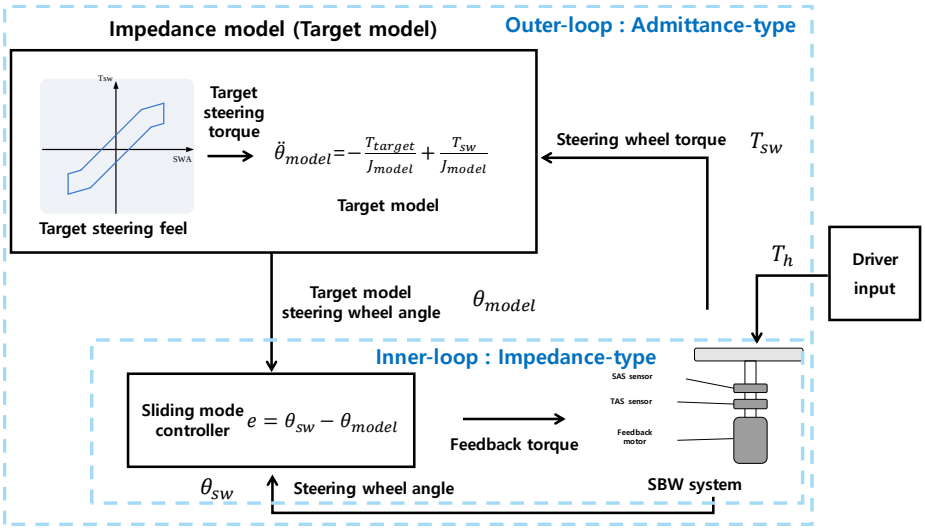

Figure 3.4 Steer-by-wire control algorithm

The steering feedback motor control algorithm consists of three parts, as shown in Figure 3.4. In the outer loop, the impedance model (Target steering model), which is in fact an admittance-type, is designed using measurement data of the target vehicle. The steering states are estimated to implement the adaptive sliding-mode control using the Kalman filter as mentioned above. In the inner loop, on the other hands, the adaptive sliding-mode controller, which is nonlinear impedance-type torque controller, is used for the target steering model tracking. Simultaneously, in the outer, the estimation of uncertain

parameters is obtained to employ in the inner loop impedance controller.

The target steering model is constructed using the steering characteristics of the vehicle with conventional steering systems. Vehicles with conventional steering systems are difficult to create the desired steering feel due to disturbances from tires. SBW systems, on the other hand, are simple enough to create the steering feel that makers want because of their simple structure. Therefore, using the three-dimensional torque map (Figure 3.1) presented above, the target model was constructed as follows:

$$J_{model}\ddot{\theta}_{model} + T_{map}\left(\dot{\theta}_{model}, \theta_{model}, V\right) = T_{sw} \tag{3.24}$$

where J_{model} and θ_{model} are the target model moment of inertia and the target model angle, respectively; T_{map} is the torque of the three-dimensional torque map; V is the vehicle speed, and T_{sw} is driver steering wheel torque measured from the torque senor in steering wheel system. If a driver's steering torque is applied to the steering wheel, the target model steering wheel states which has inertia and desired torque map is operated at a certain steering angle. And steering states of target model are calculated. Using these states from the target model, a controller to track the target model angle will be proposed.

The control algorithm for the previously proposed EPS is complicated because there is disturbance coming from the tire. On the other hand, when designing

the controller for the SBW control algorithm, it can be developed by the equation except the tire force. Similar to the EPS, the second-order model with the added friction model is as follows:

$$\begin{aligned}&\left(\hat{J}_{eq}+\Delta J_{eq}\right)\ddot{\theta}_{sw}+\left(\hat{B}_{eq}+\Delta B_{eq}\right)\dot{\theta}_{sw}+\left(\hat{T}_{friction}+\Delta T_{friction}\right)\tanh\left(\dot{\theta}_{sw}\right)\\&=T_{sw}+T_{mot}+\Delta_{un}\end{aligned}\tag{3.25}$$

where the hat, $\hat{}$, of a signal represents the nominal value, and the delta, Δ , represents the unmodeled term of the steering-wheel system. The matching condition can be approximated by:

$$\hat{J}_{eq}\ddot{\theta}_{sw}+\hat{B}_{eq}\dot{\theta}_{sw}+\hat{T}_{friction}\tanh\left(\dot{\theta}_{sw}\right)=T_{sw}+T_{mot}+L\left(t\right)\tag{3.26}$$

where $L(t)$ is the lumped uncertainty, which is unknown. However, $L(t)$ is bounded

$$\left|L\left(t\right)\right|=\left|\Delta J_{eq}\ddot{\theta}_{sw}+\Delta B_{eq}\dot{\theta}_{sw}+\Delta T_{friction}\tanh\left(\dot{\theta}_{sw}\right)-\Delta_{un}\right|<L_{m}\tag{3.27}$$

where L_m is a positive real constant.

The sliding surface, $s(t)$ has been defined as a linear combination of the steering-wheel angle error, $e(t)$ and the derivative of error as follows:

$$
\begin{aligned}
s(t) &= e(t) + \lambda \dot{e}(t) \\
e(t) &= \theta_{sw}(t) - \theta_{model}(t)
\end{aligned}
\tag{3.28}
$$

where e is the error between the steering-wheel angle and the target model angle; λ is a positive gain; and s is a sliding variable. The appropriate gain is selected to improve performance. The control input is obtained from the derivative of the sliding variable.

$$
\begin{aligned}
\dot{s}(t) &= \dot{e} + \lambda\left(\ddot{\theta}_{sw} - \ddot{\theta}_{model}\right) \\
&= \dot{e} + \frac{\lambda}{J_{model}}\left[J_{eq}\ddot{\theta}_{sw} - J_{model}\ddot{\theta}_{model} + \left(J_{model} - J_{eq}\right)\ddot{\theta}_{sw}\right] \\
&= \dot{e} + \frac{\lambda}{J_{model}}\begin{bmatrix} -B_{eq}\dot{\theta}_{sw} - T_{friction}\tanh\left(\dot{\theta}_{sw}\right) + T_{mot} + T_{map} \\ +\left(J_{model} - J_{eq}\right)\ddot{\theta}_{sw} + \Delta_{un} \end{bmatrix} \\
u_{eq} &= -T_{map} + \hat{B}_{eq}\dot{\theta}_{sw} + \hat{T}_{friction}\tanh\left(\dot{\theta}_{sw}\right) + \left(\hat{J}_{eq} - J_{model}\right)\ddot{\theta}_{sw} - \frac{J_{model}}{\lambda}\dot{e}
\end{aligned}
\tag{3.29}
$$

where u_{eq} is the equivalent control input. In order to compensate for the lumped uncertainty, a switching control input u_N is introduced, as follows:

$$
u_N = k\ \mathrm{sat}\left[s(t)/\Phi\right] \tag{3.30}
$$

where k is a positive gain satisfying $L_m < k$; Φ refers to the thickness of the boundary layer that affects the chattering solution and steady-state accuracy; and $\mathrm{sat}\left[s(t)/\Phi\right]$ denotes the saturation function:

$$\text{sat}\left[s(t)/\Phi\right] = \begin{cases} 1 & if\ \ s(t) > \Phi \\ -1 & if\ \ s(t) < -\Phi \\ s(t)/\Phi & else \end{cases} \tag{3.31}$$

Finally, the total control input u is as defined by:

$$u = T_{mot} = u_{eq} + u_N \tag{3.32}$$

However, there are parametric uncertainties. In order to compensate for these uncertainties in equivalent control input, adaptation laws must be introduced. Then, to obtain the adaptation laws, a Lyapunov function $V(t)$ is used as follows:

$$V = \frac{1}{2}s^2 + \frac{1}{2}\rho_1 \Delta J_{eq}{}^2 + \frac{1}{2}\rho_2 \Delta B_{eq}{}^2 + \frac{1}{2}\rho_3 \Delta T_{friction}{}^2 \tag{3.33}$$

As in the case of the EPS algorithm, the following adpatation law can be obtained:

$$\begin{aligned} \hat{J}_{eq} &= -\frac{\lambda}{\rho_1 J_{model}} s \cdot \ddot{\theta}_{sw} \\ \hat{B}_{eq} &= -\frac{\lambda}{\rho_2 J_{model}} s \cdot \dot{\theta}_{sw} \\ \hat{T}_{friction} &= -\frac{\lambda}{\rho_3 J_{model}} s \cdot \tanh\left(\dot{\theta}_{sw}\right) \end{aligned} \tag{3.34}$$

Since we assumed that the positive gain k is larger than the unmodeled term

(Δ_{un}), the derivative of the Lyapunov function is proved to be negative. Therefore, the system with this control input is asymptotically stable.

Chapter 4 Validation with Simulation and Hardware-in-the-Loops Simulation

4.1. Computer Simulation Results for EPS system

Computer simulations were conducted with Matlab/Simulink and Carsim co-simulation to evaluate the proposed EPS torque control algorithm using adaptive sliding mode control. Weave and transition open-loop tests have been performed to investigate the performance of the proposed algorithm. The weave and transition tests are simulated on a dry road (friction coefficient, 0.85). Open-loop command determines the steering wheel angle. In case of weave, the steering wheel angle input is 30 deg, 0.3 Hz. The vehicle speed is set to constant 60 km/h. In case of transition, the steering wheel angular velocity input is 5 deg/s. The vehicle speed is also set to constant 60 km/h.

Figure 4.1 shows the weave simulation results. Figure 4.1 (a) shows the steering wheel angle input. Figure 4.1 (b) shows the control input current from the controller. Figure 4.1 (c) presents the steering wheel torque with respect to steering wheel angle. The reference is the target steering wheel torque from the

target steering wheel torque map and the actual is the steering wheel torque of a driver. It was observed that the actual tracked the target well. Figure 4.1 (f) also shows the tracking error plot between the steering wheel torque and the target steering wheel torque. Time histories of the three adaptation parameters, the moment of inertia, $\hat{J}_{eq}$, the damping coefficient, $\hat{B}_{eq}$, and the effective compliance, $\hat{K}_{eff}$, are shown in Figure 4.1 (d). The moment of inertia and damping coefficient show that there is not much variation in time because the values are known in advance as system parameters. However, the effective compliance varied according to the situation. Figure 4.1 (e) shows the actual rack force compared with nominal rack force, $\hat{F}_r$, and adapted rack force. The adapted rack force is the sum of the nominal rack force and the effective compliance force, $\hat{K}_{eff}\theta_{sw} / R_{rp}$. It can be seen that the adapted rack force tracks the actual rack force well.

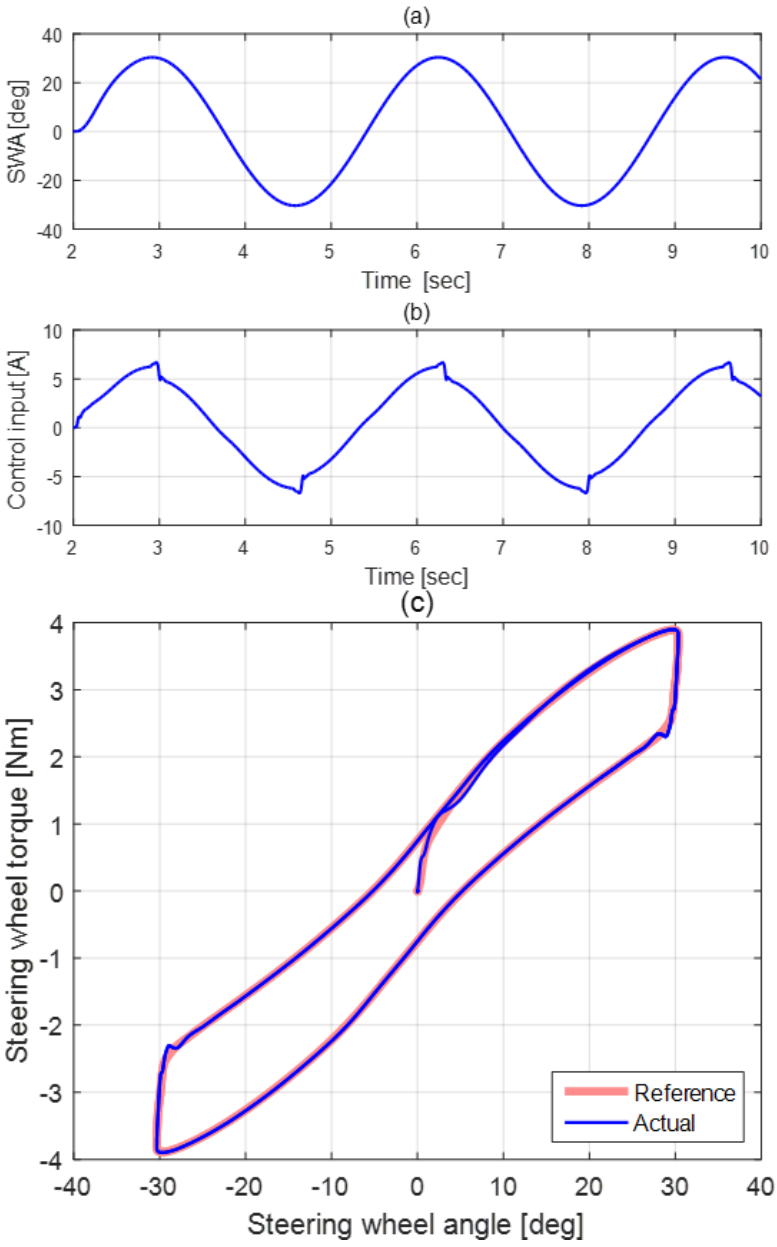
(a)
SWA [deg]
Time [sec]
(b)
Control input [A]
Time [sec]
(c)
Steering wheel torque [Nm]
Steering wheel angle [deg]
Reference
Actual

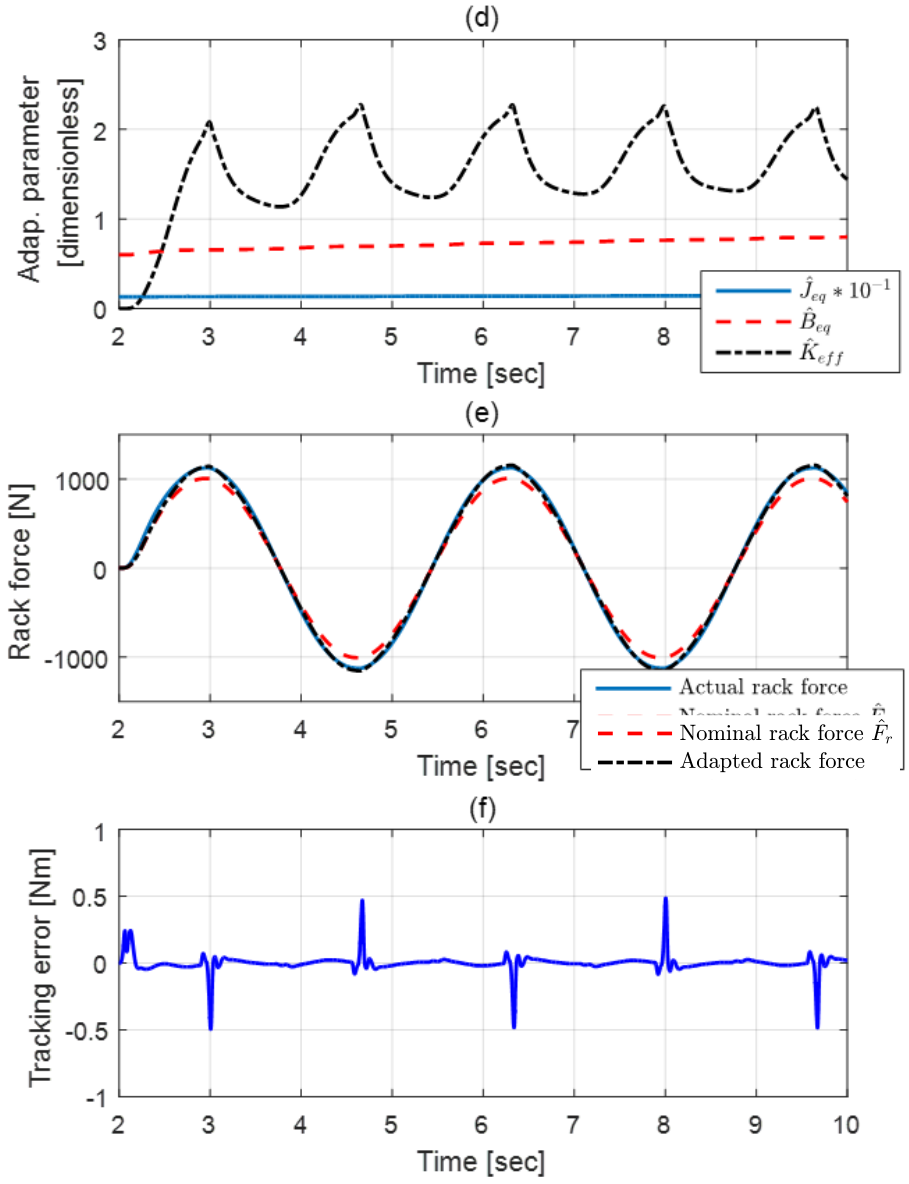

Figure 4.1 30deg weave test at 60km/h.

Figure 4.2 shows the transition test results. As above weave test, Figure 4.2 (a)-(f) show steering wheel angle, control input, steering wheel torque with respect to steering wheel angle, adaptation parameters, rack forces, and tracking error. As shown in Figure 4.2 (c), it was also observed that the actual tracked the target well. The actual rack force, nominal rack force, $\hat{F}_r$, and adapted rack force as shown in Figure 4.2 (e). The adapted rack force is the sum of the nominal rack force and the effective compliance force, $\hat{K}_{eff}\theta_{sw} / R_{rp}$. It can be seen that the adapted rack force tracks the actual rack force well as above weave simulation.

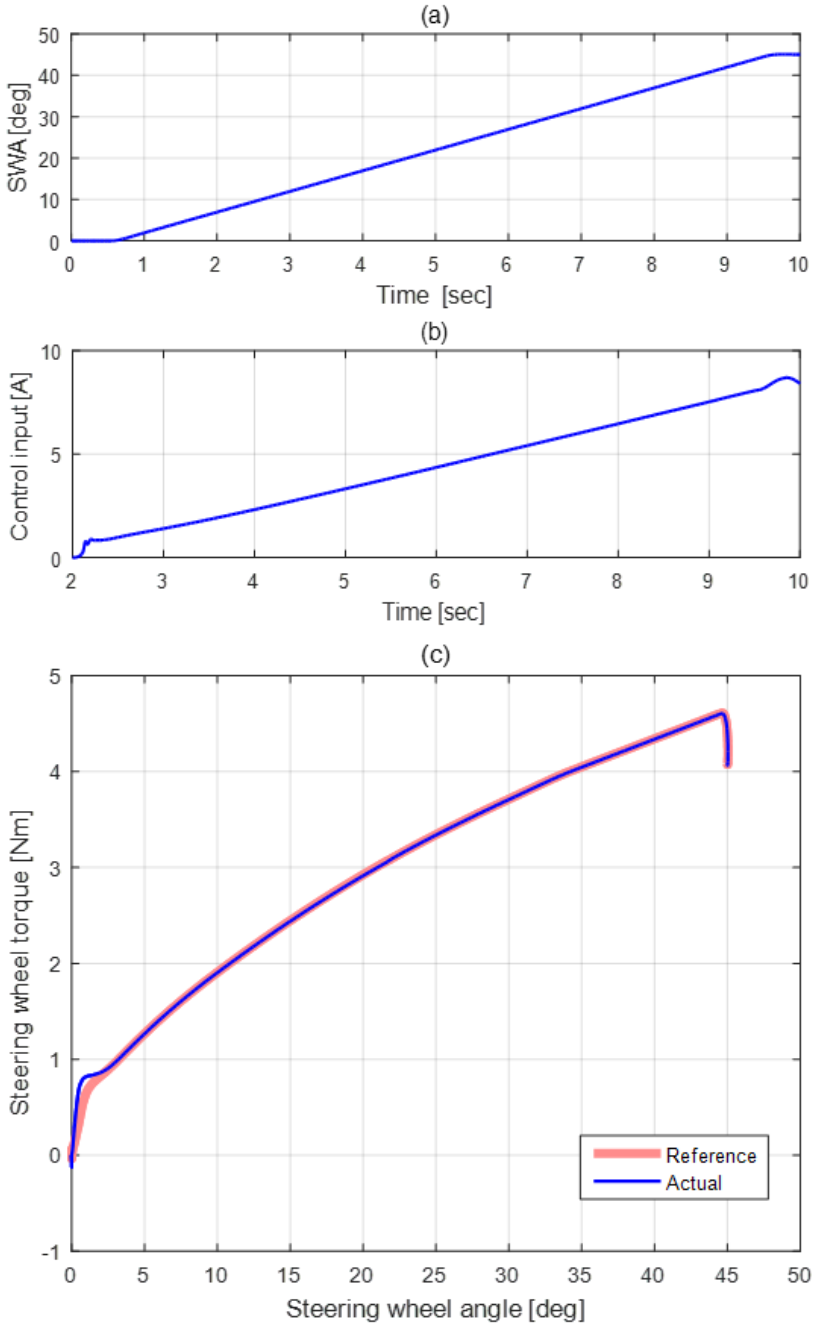
(a)
SWA [deg]
Time [sec]
(b)
Control input [A]
Time [sec]
(c)
Steering wheel torque [Nm]
Steering wheel angle [deg]
Reference
Actual

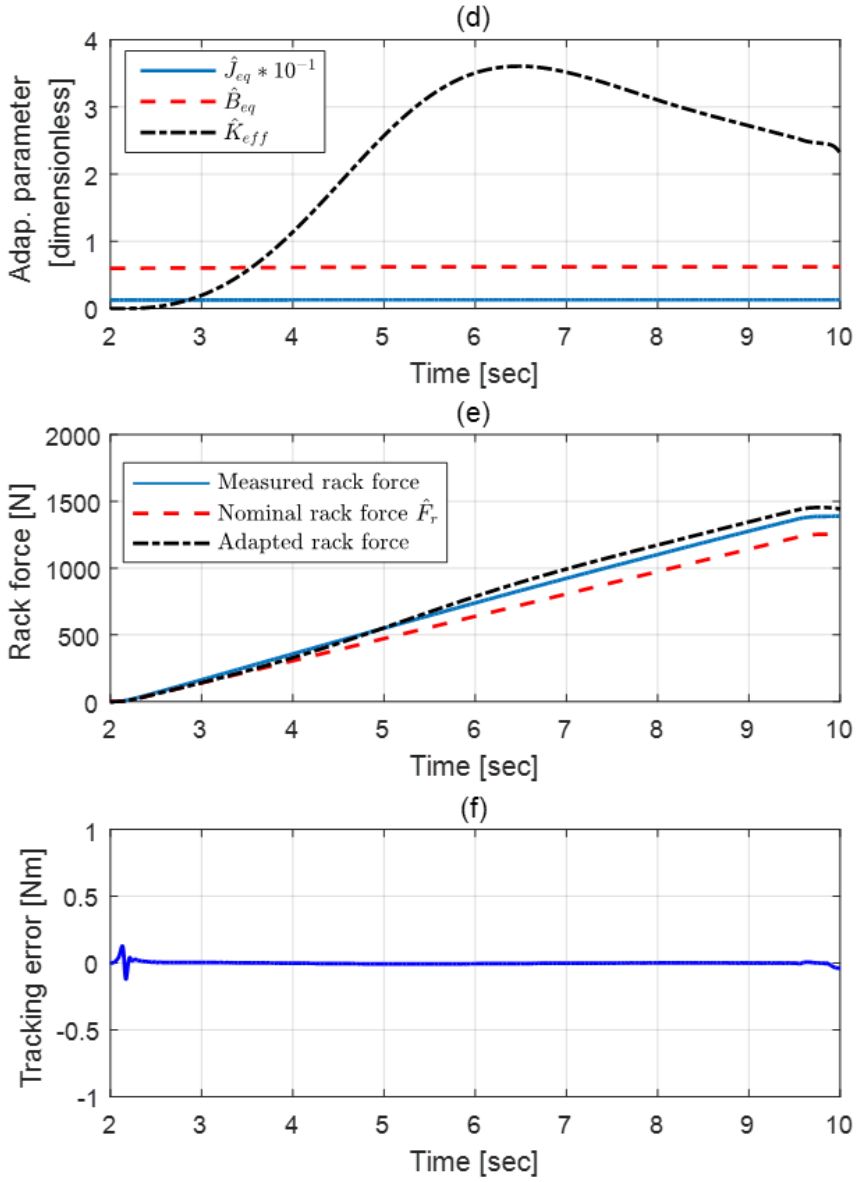

Figure 4.2 5deg/s transition test at 60km/h.

A comparison of the proposed ASMC with PID 1 (P=2, I=200, D=0.03) and PID 2 (P=2, I=100, D=0.03) control is conducted on the weave test to investigate the steering wheel torque tracking performance. The simulation is conducted with a 60 kph, 30 deg steering wheel angle input with 0.3 Hz. As can be seen in Figure 4.3(e), the ASMC has the smallest steady-state error of these. A PID 1 simulation is conducted to reduce the steady-state error using a larger I gain than that for PID 2. Although the steady-state error for PID 1 has been reduced, this case has a more massive oscillation than PID 2. The reason for this is that the steering wheel torque tracking error increased abruptly during the return, as shown in Figure 4.3 (e). Therefore, an oscillation occurs if a larger gain was adopted. In contrast, the proposed ASMC tracks the target steering wheel torque well in all situations, as seen in Figure 4.3 (e) for the ASMC.

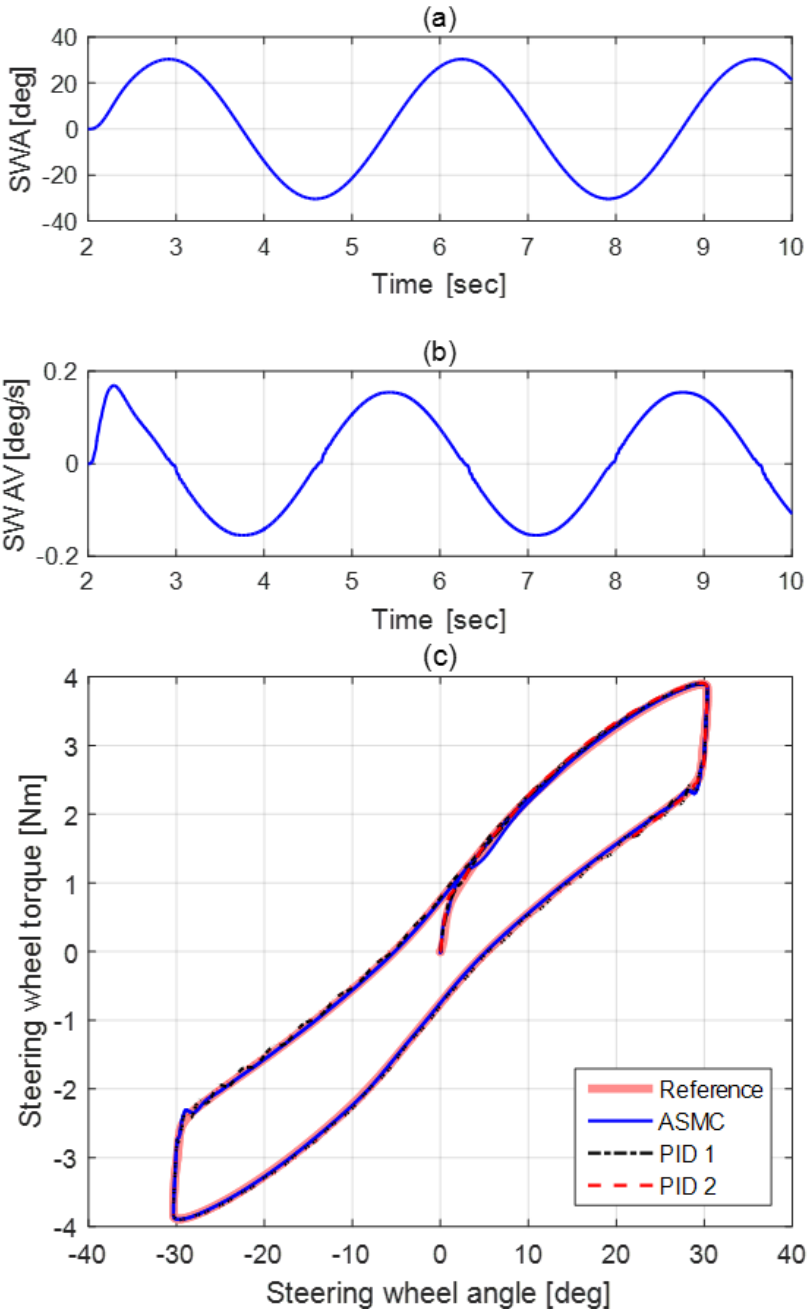
(a)
SWA [deg]
40
20
0
-20
-40
2
3
4
5
6
7
8
9
10
Time [sec]
(b)
SW AV [deg/s]
0.2
0
-0.2
2
3
4
5
6
7
8
9
10
Time [sec]
(c)
Steering wheel torque [Nm]
4
3
2
1
0
-1
-2
-3
-4
-40
-30
-20
-10
0
10
20
30
40
Steering wheel angle [deg]
Reference
ASMC
PID 1
PID 2

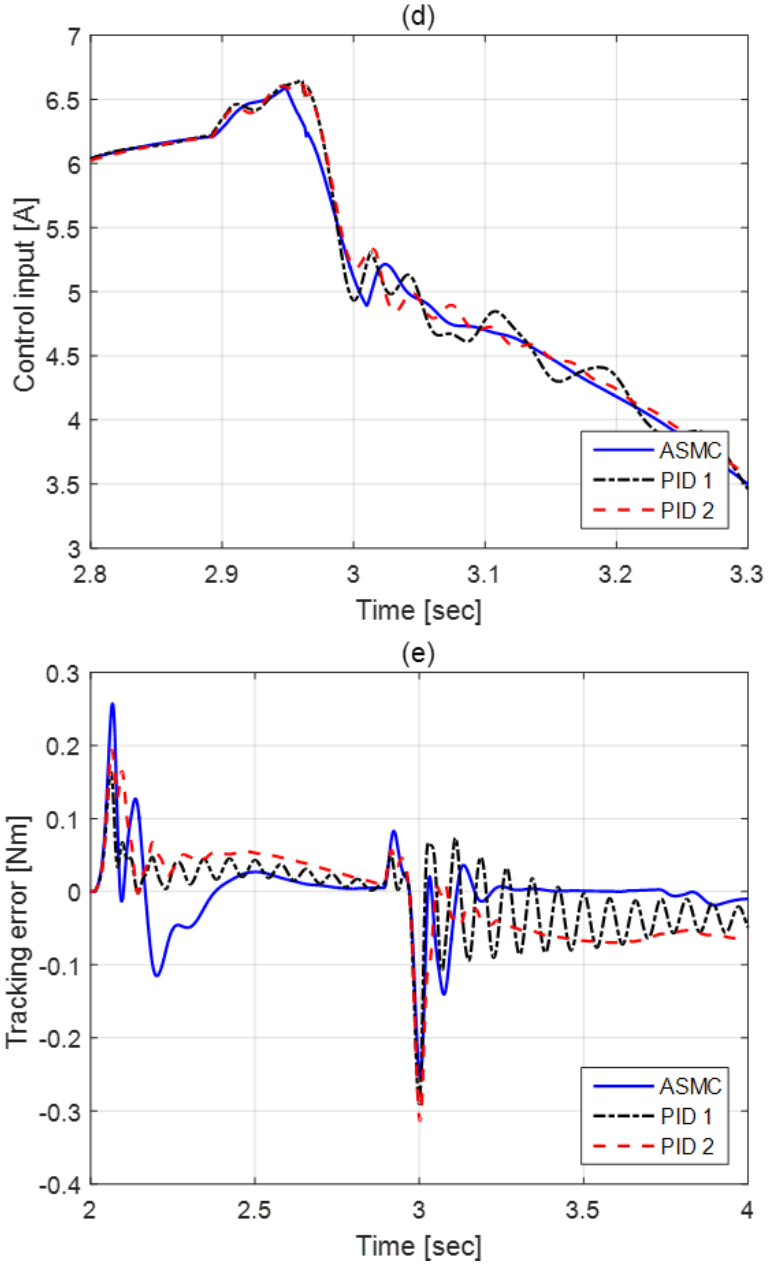

Figure 4.3 Comparison of the proposed ASMC with PID control.

The nominal rack force, $\hat{F}_r$, varies from 50% to 150% to analyze the robustness of the performance with respect to the nominal rack force parameter. The calculated value from Eq. (19) depicts the reason behind the changing toe nominal rack. However, this may be inaccurate due to parameter uncertainties, such as pneumatic trail, mechanical trail, steering arm length, and lateral tire stiffness uncertainty. All other conditions are identical to those in the above simulation. Figure 4.4 shows the root mean square (RMS) tracking error between the steering wheel torque and the target steering wheel torque with respect to $\hat{F}_r$ for the presence and absence of the adaption. The variation in performance for the presence of the adaptation is much smaller than that with the absence. These results imply that the proposed adaptation sliding model control is very useful in tracking steering wheel torque against parameter uncertainty.

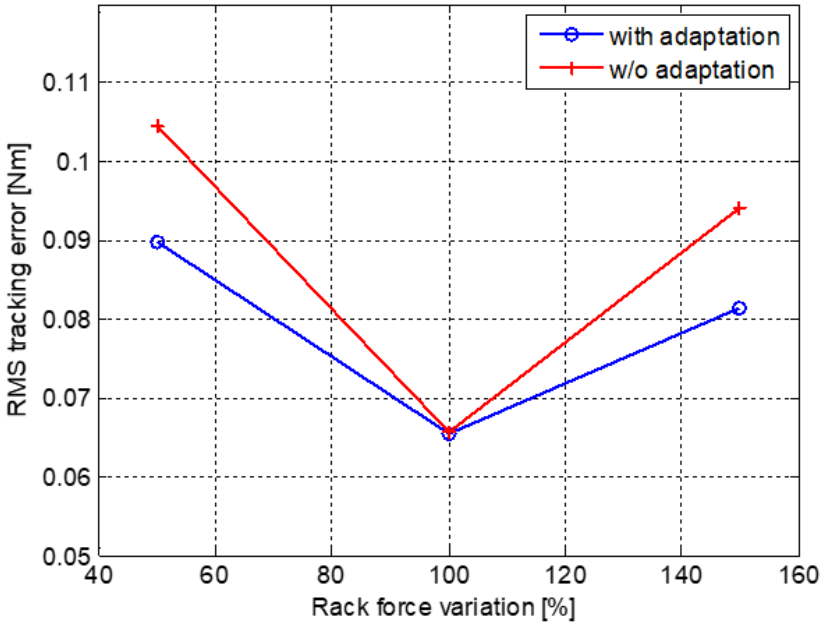

Figure 4.4 Comparison of the RMS tracking error with and without adaptation.

4.2. Hardware-in-the-Loops Simulation Results for EPS system

The proposed control algorithm was investigated by the hardware-in-the-loop-simulation (HILS). As shown in Figure 4.5, the HILS consists of two parts: a software part and a hardware part. In the software part, Carmaker from IPG Automotive was used to implement the full vehicle dynamics model using the real-time simulator (DS1006) from dSPACE and micro-autobox (1401/1511/1513) to implement the proposed EPS control algorithm from dSPACE. The hardware part comprises five components. The steering robot generates the accurate steering input. The hydraulic cylinder unit (maximum output 15-kilonewton) from MTS Systems Corporation creates the rack force from the vehicle model. EPS ECU controls the motor using the current input from the proposed algorithm. The rack displacement sensor is transferred to the dynamic model by measuring the displacement rack. The TAS sensor measures the torque and angle, and transmits the information to the autobox.

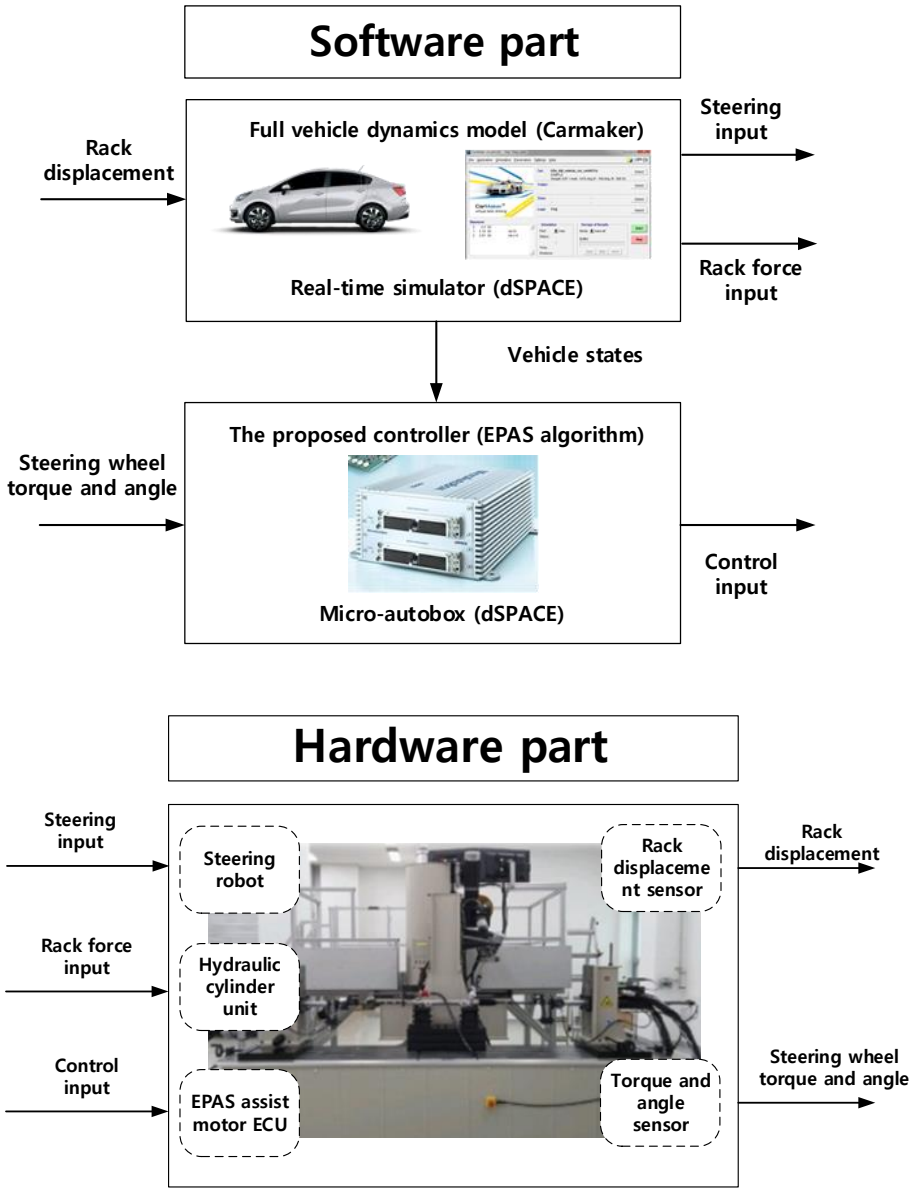

Figure 4.5 Schematic diagram of the hardware-in-the-loop-simulation (HILS).

As previously conducted with the computer simulation, the weave and transition tests are simulated on a dry road (friction coefficient, 0.85). Open-loop command determines the steering wheel angle, as the above computer simulation tests. In the case of weave, the steering wheel angle input is 30 deg and 0.3 Hz. The vehicle speed is set to be constant at 60 km/h. In the case of transition, the steering wheel angular velocity input is 5 deg/s. The vehicle speed is also set to be constant at 60 km/h.

Figure 4.6 shows the HILS results of the weave test. The results of the HILS simulation are arranged in parallel with the results in Figure 4.6 of the computer simulation. It was also observed that the actual tracked the reference well, as shown in Figure 4.6 (c) and (f). Unlike the computer simulation, in the weave test, effective compliance was slightly smoother, as shown in Figure 4.6 (d). The adapted rack force tracks the actual rack force well, as with the computer simulation in Figure 4.6 (e). As the effective compliance changed, it can be seen that the error gradually decreased, as shown in Figure 4.6 (f).

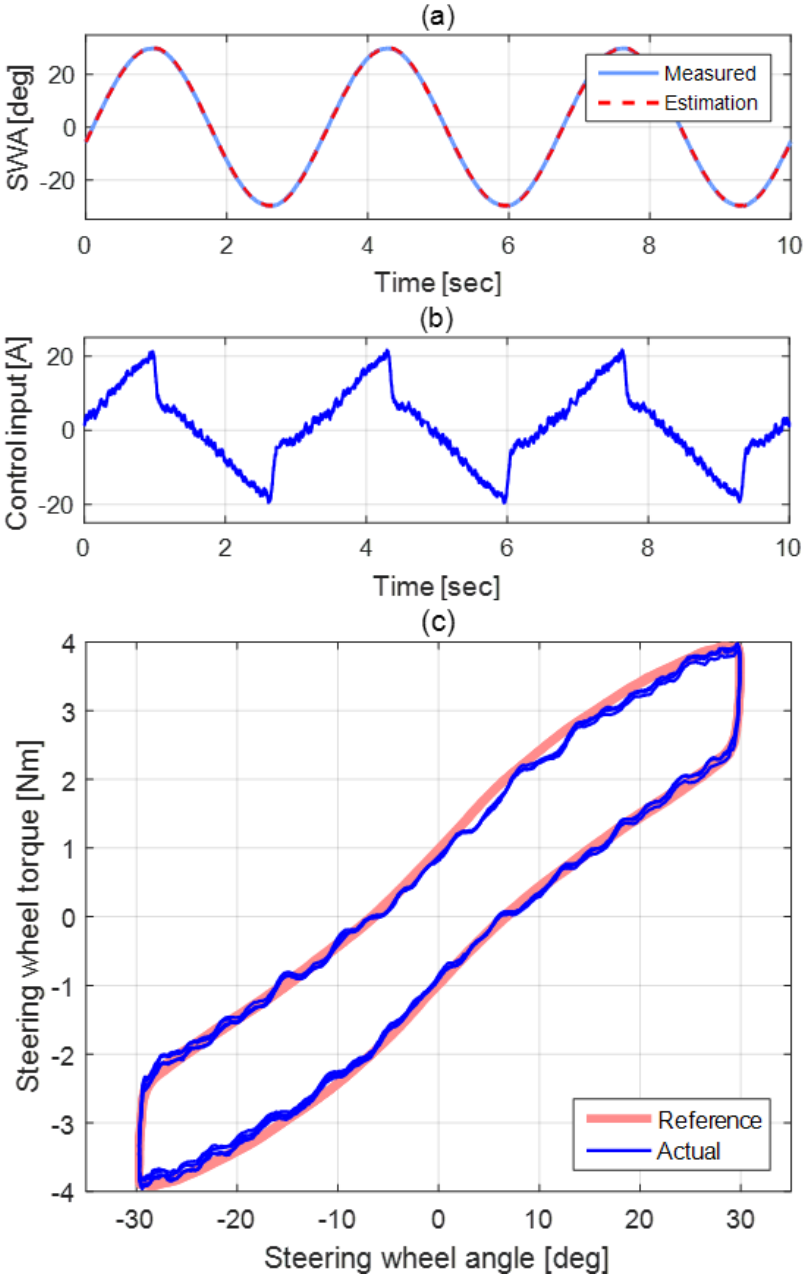
(a)
SWA [deg]
20
0
-20
0
2
4
6
8
10
Time [sec]
Measured
Estimation
(b)
Control input [A]
20
0
-20
0
2
4
6
8
10
Time [sec]
(c)
Steering wheel torque [Nm]
4
3
2
1
0
-1
-2
-3
-4
-30
-20
-10
0
10
20
30
Steering wheel angle [deg]
Reference
Actual

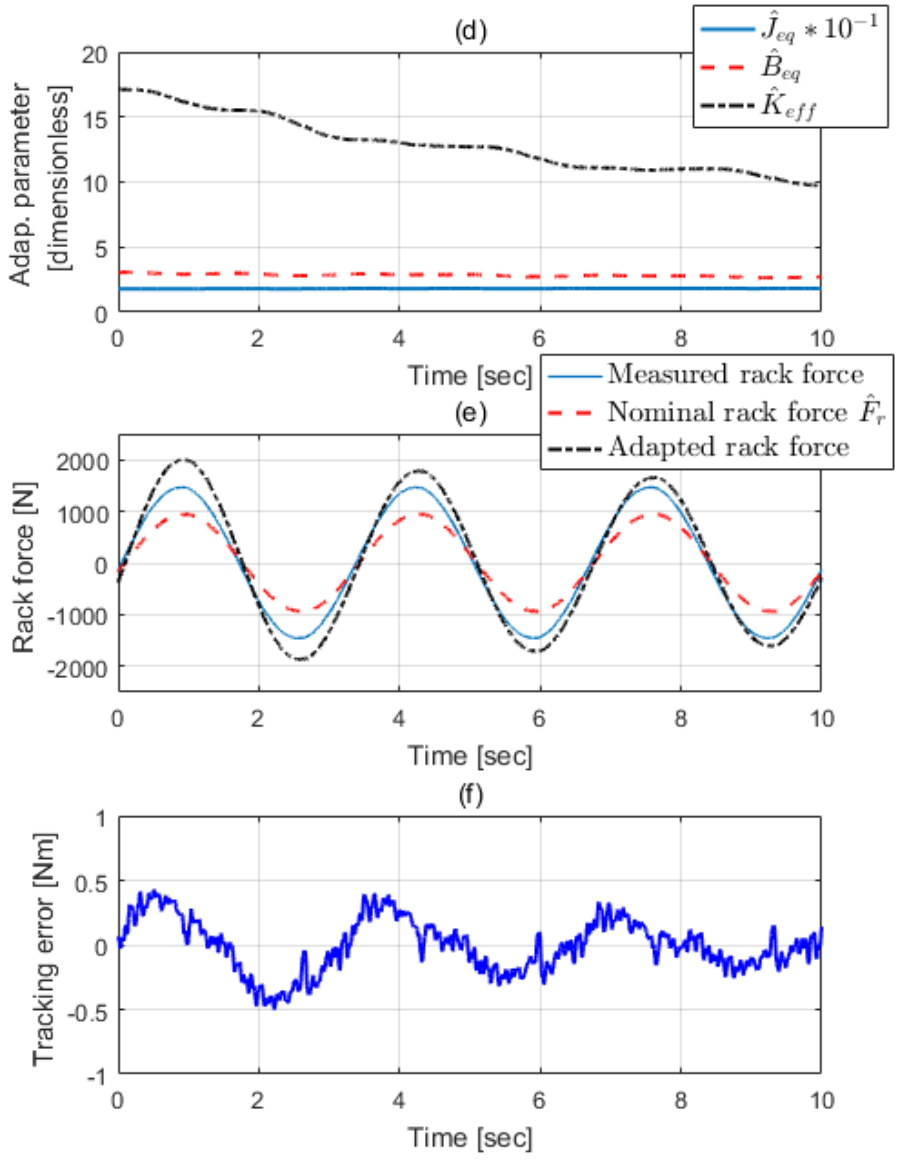

Figure 4.6 30 deg weave test at 60 km/h.

Fig. 12 shows the HILS transition test results. The results of the HILS simulation are arranged in parallel with the results in Fig. 7 of the computer simulation. It was also observed that the actual tracked the reference well, as shown in Fig. (c) and (f). In addition, it can be seen that the adapted rack force tracked the actual rack force well, as shown in Fig. (e). Although the equivalent moment of inertia, $\hat{J}_{eq}$, the equivalent damping, $\hat{B}_{eq}$, and the effective compliance, $\hat{K}_{eff}$, are chosen as adaptation parameters to guarantee robustness to parameter uncertainty, it was confirmed that the effective compliance was dominant compared to others, as can be seen in the above results.

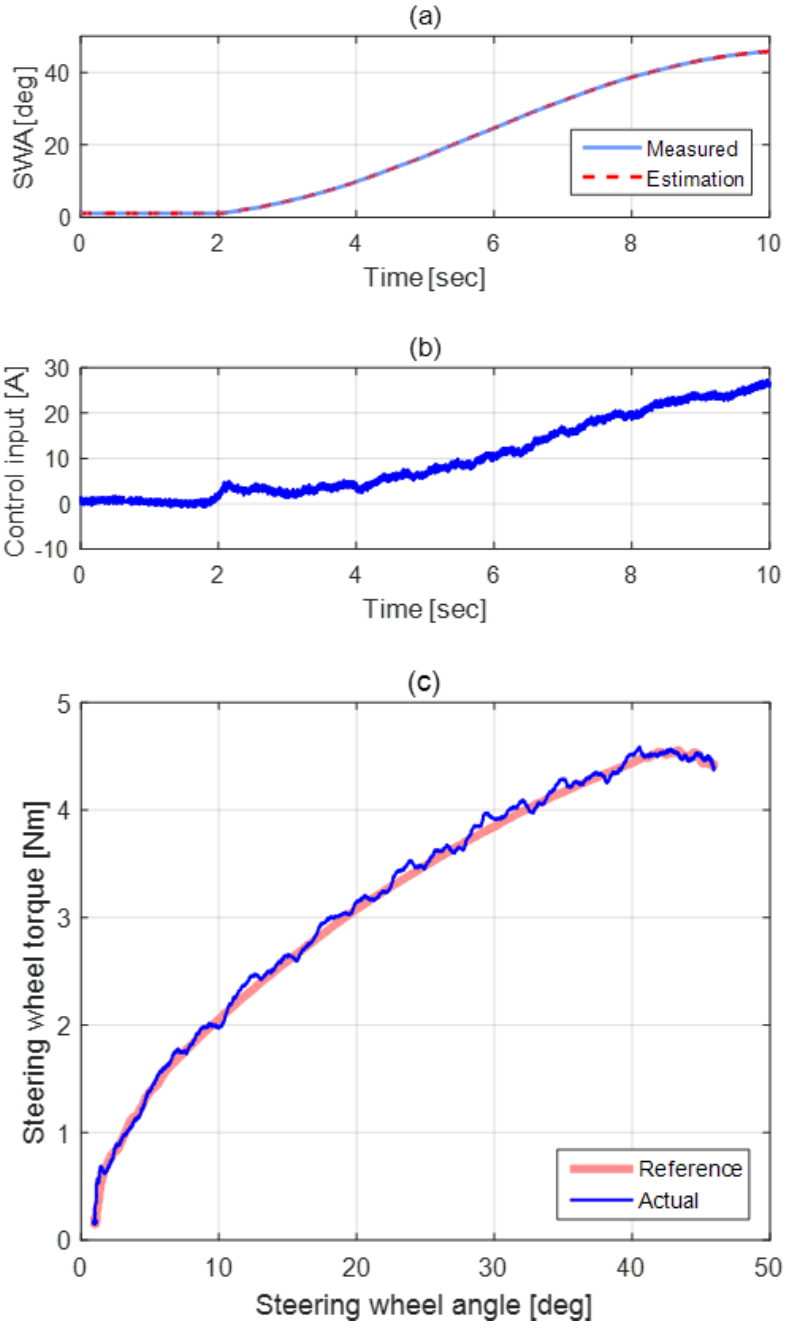
(a)
SWA [deg]
40
20
0
0
2
4
6
8
10
Time [sec]
Measured
Estimation
(b)
Control input [A]
30
20
10
0
-10
0
2
4
6
8
10
Time [sec]
(c)
Steering wheel torque [Nm]
5
4
3
2
1
0
0
10
20
30
40
50
Steering wheel angle [deg]
Reference
Actual

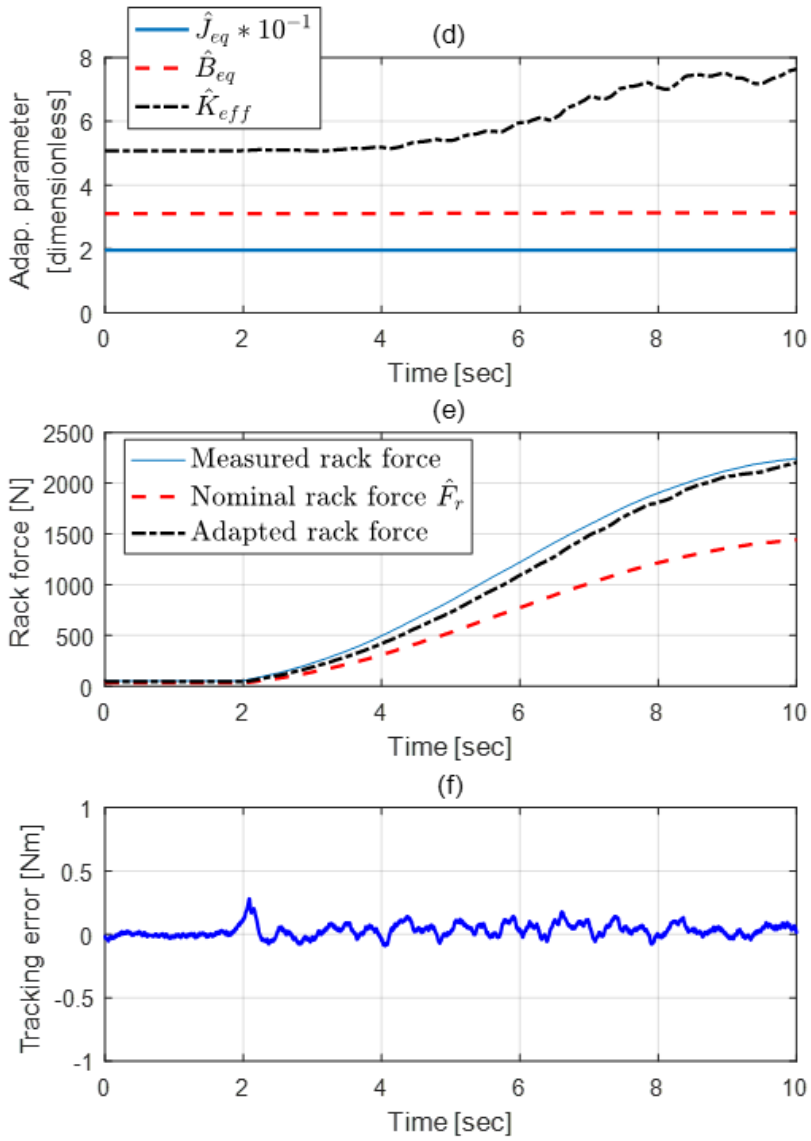

Figure 4.7 5 deg/s transition test at 60 km/h.

According to Jang et al. (Jang, et al., 2014), the objective parameters used in the steering performance evaluation are presented. In the weave test results, the steering angle vs. steering wheel torque graph can be utilized to derive such parameters as on-center stiffness, steering friction and angle hysteresis, as can be seen in Table 2. Here, the on-center stiffness is the gradient at zero angles, the steering friction is ordinate deadband, and the angle hysteresis is abscissa deadband. In addition, average steering friction and off-center stiffness were used in the transition test results, as can be seen in Table 3. The average steering friction is average torque 0 deg to 1 deg, and the off-center stiffness is an average gradient of 5 deg to 15 deg. Computer simulation and HILS target results are different. This is because the target determined by the steering wheel angle and the angular velocity changes when the simulation environment is changed. In the weave test, the average error of the parameters of the computer simulation is approximately 4.5%, and the average error of the HILS is approximately 6.6%. In the transition test, the mean error of the parameters of the computer simulation is approximately 0.5%, and the mean error of the HILS is approximately 1.9%. The experimental results are satisfactory.

Table 2 Comparison of computer simulation and HILS results using objective parameters with the weave test.

	Unit	Computer simulation		HILS	
		Target	Actual	Target	Actual
On-center stiffness	Nm/deg	0.1577	0.1693	0.1591	0.1613
Steering friction	Nm	1.8563	1.8869	2.2316	1.8962
Angle hysteresis	deg	10.515	11.006	13.1191	12.664

Table 3 Comparison of computer simulation and HILS results using objective parameters with the transition test.

	Unit	Computer simulation		HILS	
		Target	Actual	Target	Actual
Average steering friction	Nm	0.4207	0.4172	0.5296	0.5410
Off-center stiffness	Nm/deg	0.1141	0.1142	0.1206	0.1225

Figure 4.8 presents the comparison of HILS weave test results by vehicle speed. Figure 4.8 (a) shows the steering wheel angle vs. steering wheel torque graph. In order to reflect the rack force characteristics (Figure 2.5) in the actual vehicle, the target steering wheel torque map was constructed so that the steering stiffness increases as the vehicle speed increases (40 kph : 0.1030 Nm/deg , 60 kph : 0.1591 Nm/deg , 80 kph : 0.1845 Nm/deg). On the contrary, the magnitude of the steering friction decreases with speed (40 kph : 3.4306 Nm , 60 kph : 2.2316 Nm , 80 kph : 1.427 Nm). Figure 4.8 (b) shows the error

values of the target for each speed and the steering wheel torque. It can be seen that the tracking performance is excellent. Figure 4.8 (c) presents the adapted rack force, which is the sum of the nominal rack force and the effective compliance force. Figure 4.8 (d) shows the error value between the actual rack force and the adapted rack force. The estimated performance is satisfactory.

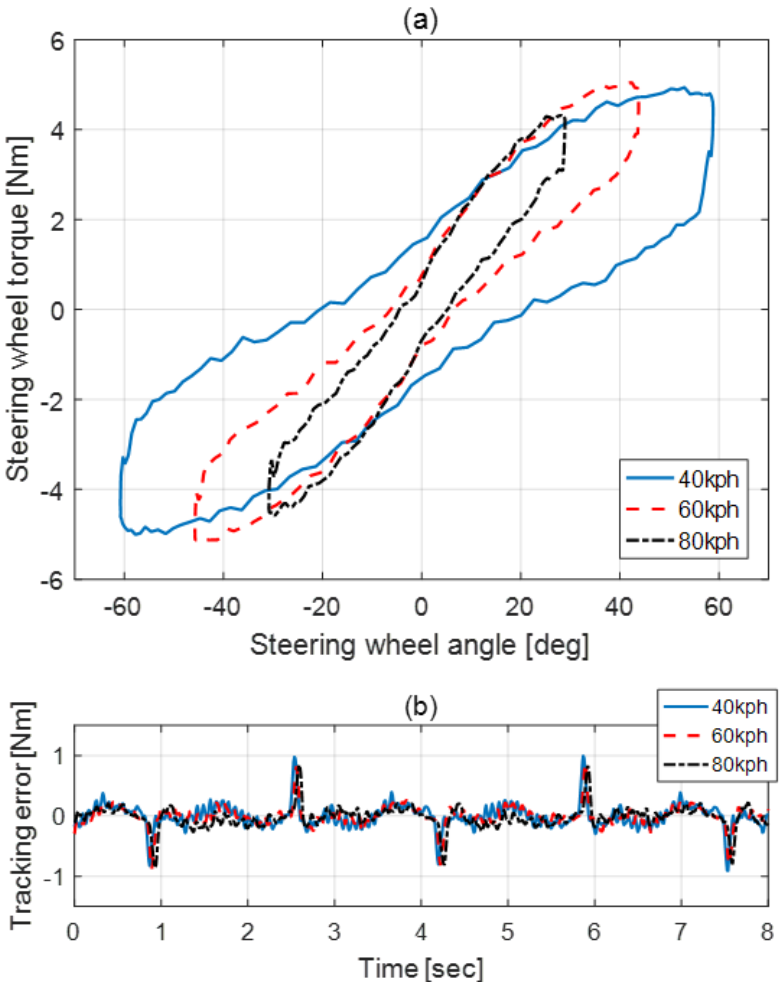

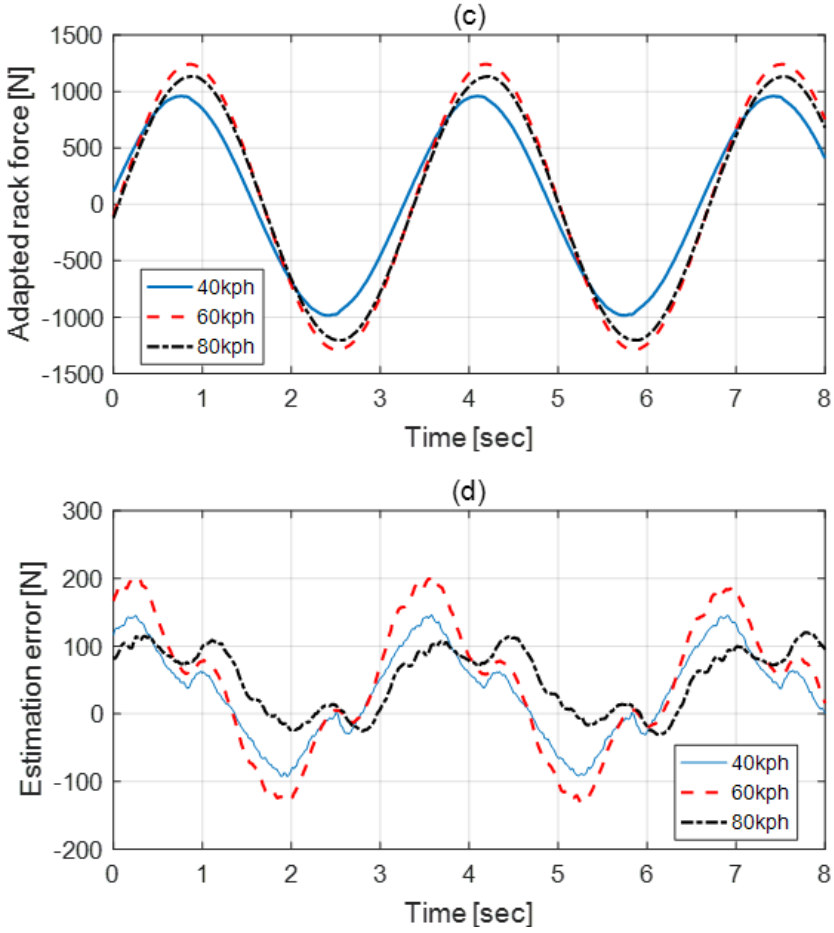

Figure 4.8 Comparison of HILS weave test results by different vehicle speeds.

Figure 4.9 shows a comparison of HILS transition test results by steering angular velocity. Figure 4.9 (a) presents the steering wheel angle. Figure 4.9 (b) shows steering wheel angle vs. steering wheel torque. The target steering wheel torque map was designed so that the average steering torque increases as the steering angular velocity increases (5 deg/s : 0.5296 Nm, 45 deg/s : 0.7784 Nm, 90 deg/s : 1.1082 Nm), and also increase the off-center stiffness (5 deg/s : 0.1206 Nm/deg, 45 deg/s : 0.1728 Nm/deg , 80 kph : 0.2045 deg/s). Figure 4.9 (c) presents the error values of the target for each speed and the steering wheel torque. It can be seen that the tracking performance is good. Figure 4.9 (d) shows the adapted rack force, which is the sum of the nominal rack force and the effective compliance force. Figure 4.9 (e) presents the error value between actual rack force and adapted rack force. The estimated performance is satisfactory.

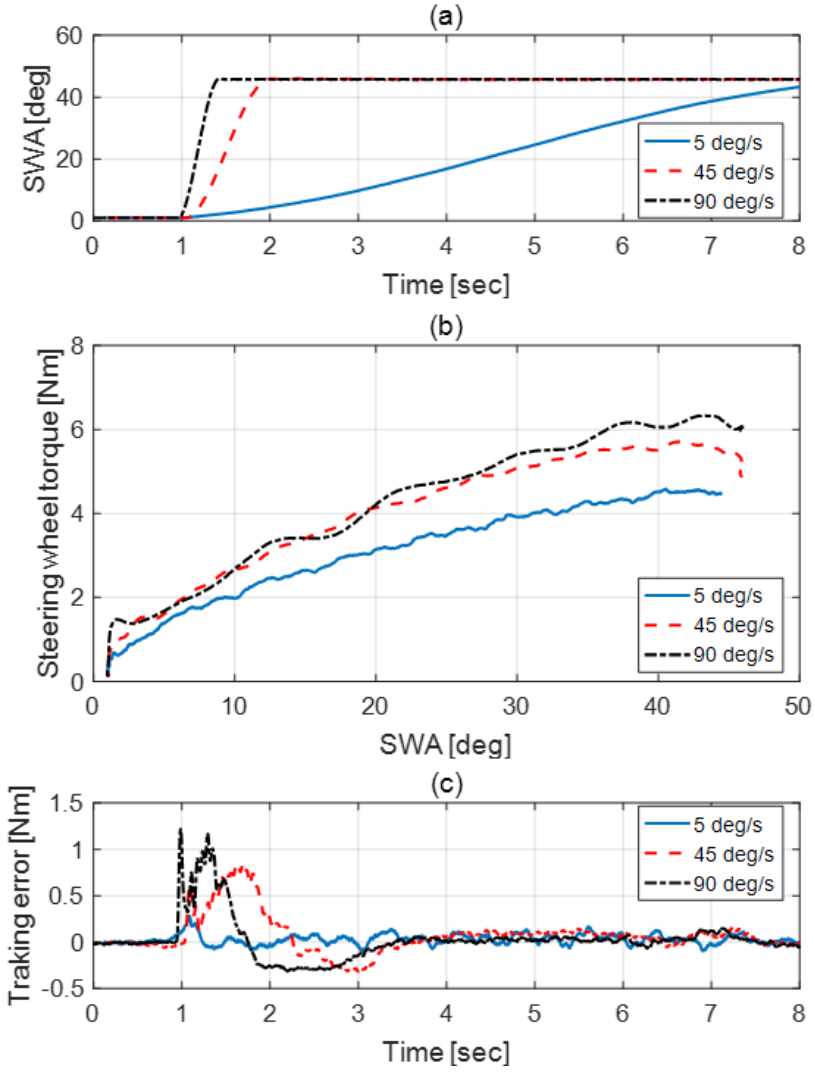
(a)
SWA [deg]
Time [sec]
5 deg/s
45 deg/s
90 deg/s
(b)
Steering wheel torque [Nm]
SWA [deg]
5 deg/s
45 deg/s
90 deg/s
(c)
Traking error [Nm]
Time [sec]
5 deg/s
45 deg/s
90 deg/s

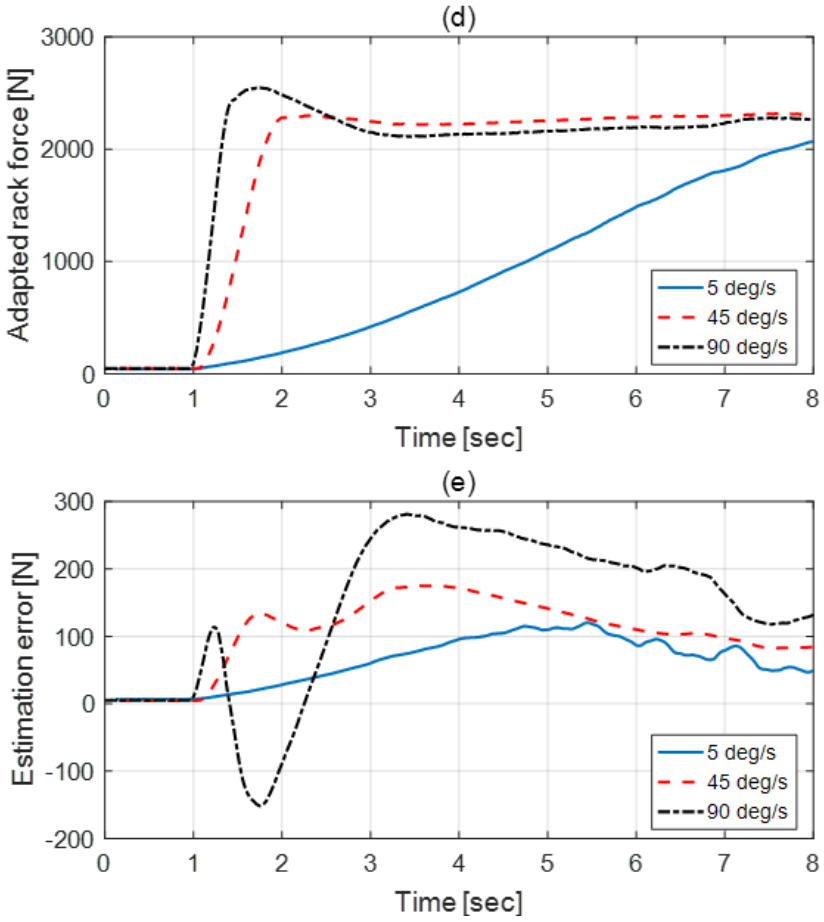

Figure 4.9 Comparison of HILS transition test results by different steering angular velocities.

4.3. Computer Simulation Results for SBW system

In this section, computer simulations are conducted to check the performance of the target steering-wheel model tracking algorithm. The steering-wheel system model was created with Matlab / Simulink. Unlike the simplified model that is used in the tracking algorithm, the steering-wheel model is composed of a DC motor, sensor stiffness, steering column inertia, and steering shaft inertia. In addition, the sensor resolution is set at 0.1 deg and the sampling time is set at 1 msec.

To validate the proposed algorithm, we have conducted the weave test and the transition test as in EPS. This study focuses on whether various targeted steering feels can be generated in a steer-by-wire system rather than on evaluating whether a good steering feel is generated.

Figure 4.10 shows the results of the weave simulation. Figure 4.10 (a) shows the steering-wheel angle. Figure 4.10 (b) shows the steering-wheel torque with respect to the steering angle. The reference is the steering-wheel torque when the steering states of the target steering system are the same as those of the actual steering system. Figure 4.10 (c) is the sliding surface. And the three adaptation parameters are illustrated in Figure 4.10 (d).

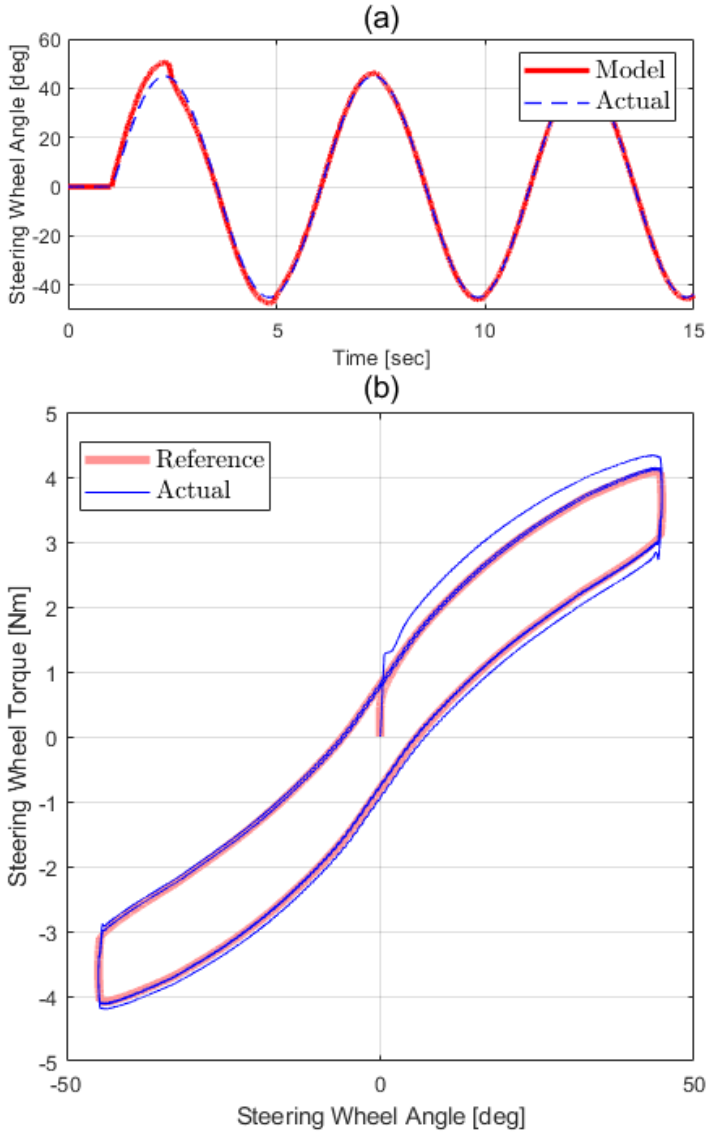
(a)
Steering Wheel Angle [deg]
60
40
20
0
-20
-40
0
5
10
15
Time [sec]
Model
Actual
(b)
Steering Wheel Torque [Nm]
5
4
3
2
1
0
-1
-2
-3
-4
-5
-50
0
50
Steering Wheel Angle [deg]
Reference
Actual

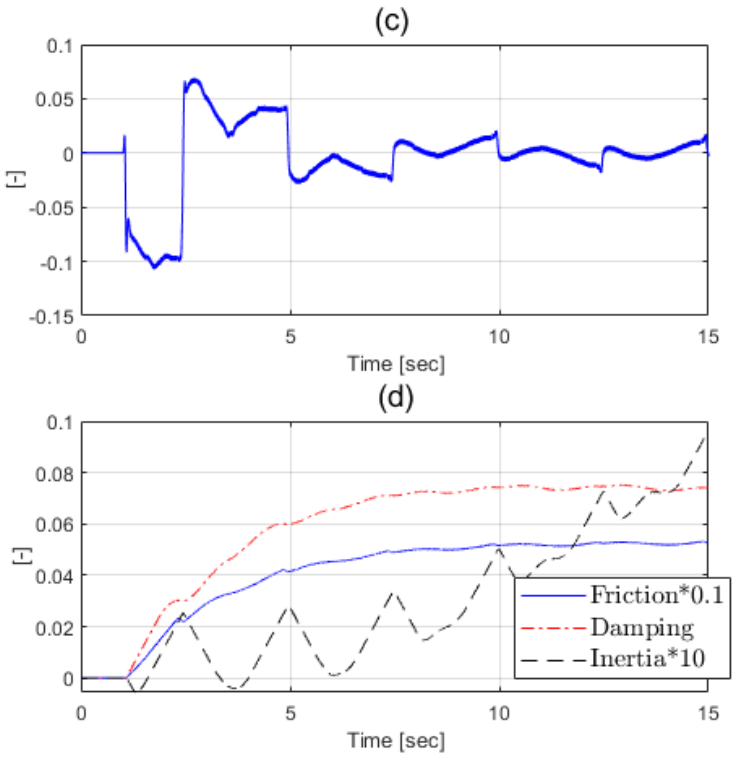

Figure 4.10 45deg weave test at 70km/h.

In this scenario, the inertia coefficient takes a long time to converge because the angular acceleration is low. After the friction coefficient and damping coefficient converge, the steering-wheel angle tracks the angle of the target steering model. Also, to the driver, the steering feel the same as in the target steering model.

Figure 4.11 shows the results of transition simulation for different target steering models. Figure 4.11 (a) presents the steering-wheel torque of Model 1 (high friction torque). Figure 4.11 (b) presents the steering-wheel torque of Model 2 (low friction torque). Figure 4.11 (c) shows the steering-wheel torque with respect to the steering angle.

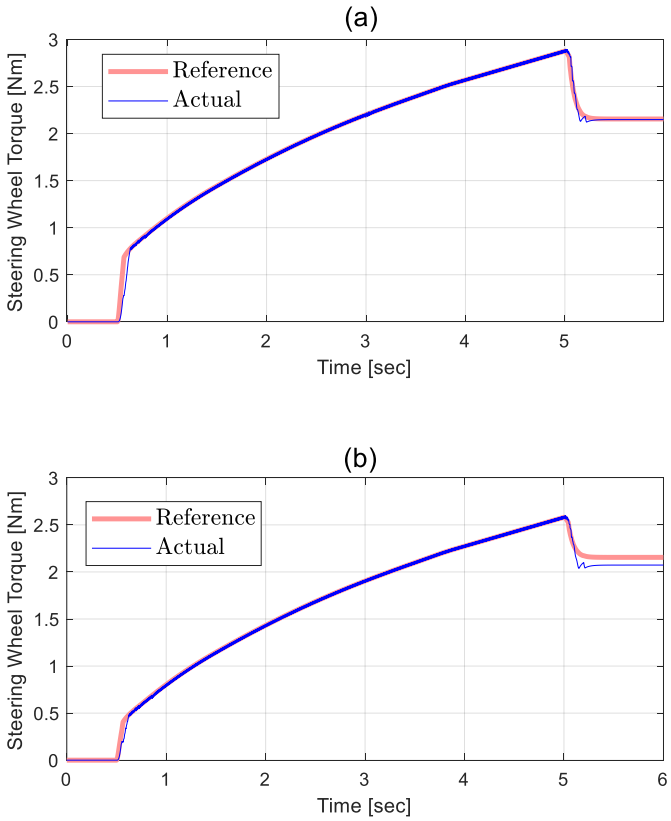

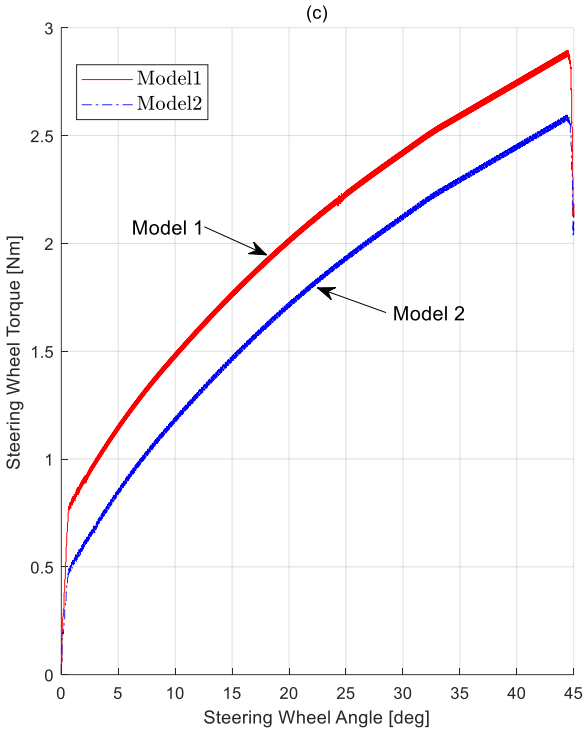

Figure 4.11 10 deg/s transition test at 70 km/h

In this scenario, it can also be seen that the steering-wheel angle tracks the angle of the target steering model and the driver has the same steering feel as in the target steering model.

4.4. Hardware-in-the-Loops Simulation Results for SBW system

The proposed control algorithm was investigated by the hardware-in-the-loop simulation (HILS). The HILS system consists of a micro-autobox and some hardware. Using the micro-autobox (1401/1511/1513), the proposed control algorithm was implemented. The hardware part comprises three components. The steering wheel is the part to which the driver applies torque. The steering feedback motor generates the steering-wheel torque to the driver. The steering sensor between the steering wheel and the steering feedback motor measures the torque and angle, and transmits the information to the autobox. Figure 4.12 is a schematic diagram of the steer-by-wire system.

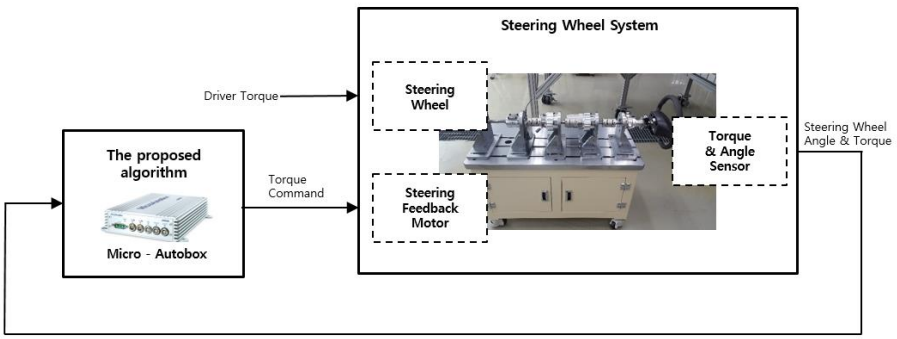

Figure 4.12 Schematic diagram of the steer-by-wire system

As previously done with the HILS test in EPS, objective parameters were

introduced to evaluate the performance of the proposed SBW algorithm.

The first scenario is the weave test. Figure 4.13 shows the results of the weave test. The results of the HILS test are arranged in parallel with the results in Figure 4.10 of the computer simulation. It can also be seen that the steering-wheel angle tracks the angle of the target steering model and the driver has the same steering feel as in the target steering model. Figure 4.14 shows the transition test results for the two steering models above. The transition test was performed at 10 deg/s. Figure 4.14 (a) presents the steering-wheel torque of Model 1, and Figure 4.14 (b) presents the steering-wheel torque of Model 2. Figure 4.14 (c) shows the steering-wheel angle vs. the steering-wheel torque. The HILS test didn't use the steering robot, and the person applied the steering-wheel torque directly, so the frequency and amplitude of the steering input were not constant, and the test was logged after adaptation parameter convergence. It was also observed that the actual steering-wheel angle tracked the target well.

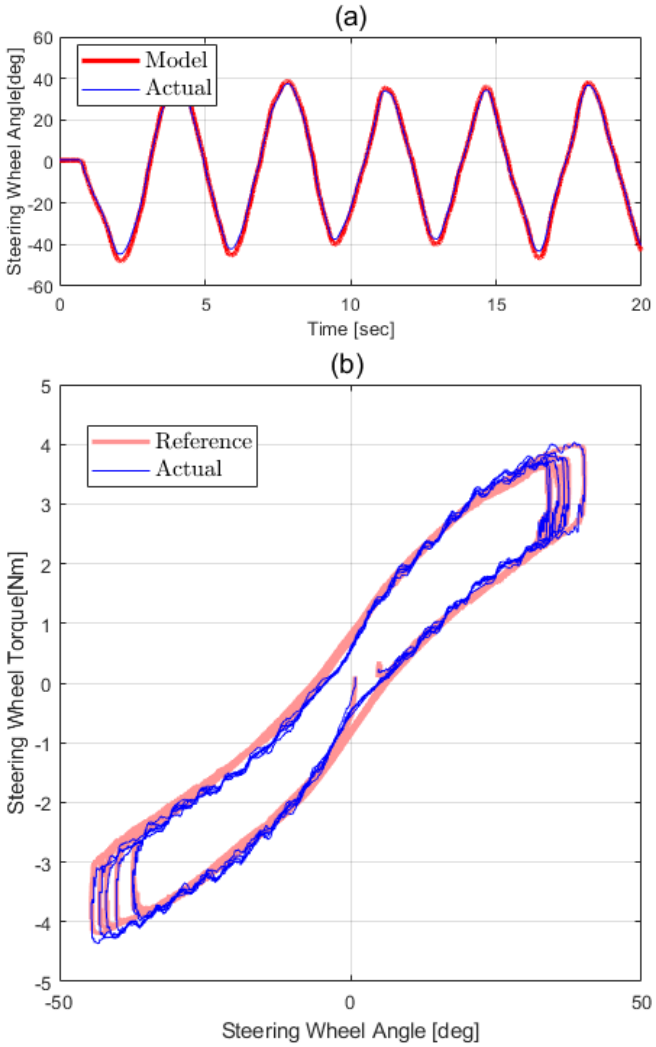
(a)
Model
Actual
Steering Wheel Angle[deg]
60
40
20
0
-20
-40
-60
0
5
10
15
20
Time [sec]
(b)
Reference
Actual
Steering Wheel Torque[Nm]
5
4
3
2
1
0
-1
-2
-3
-4
-5
-50
0
50
Steering Wheel Angle [deg]

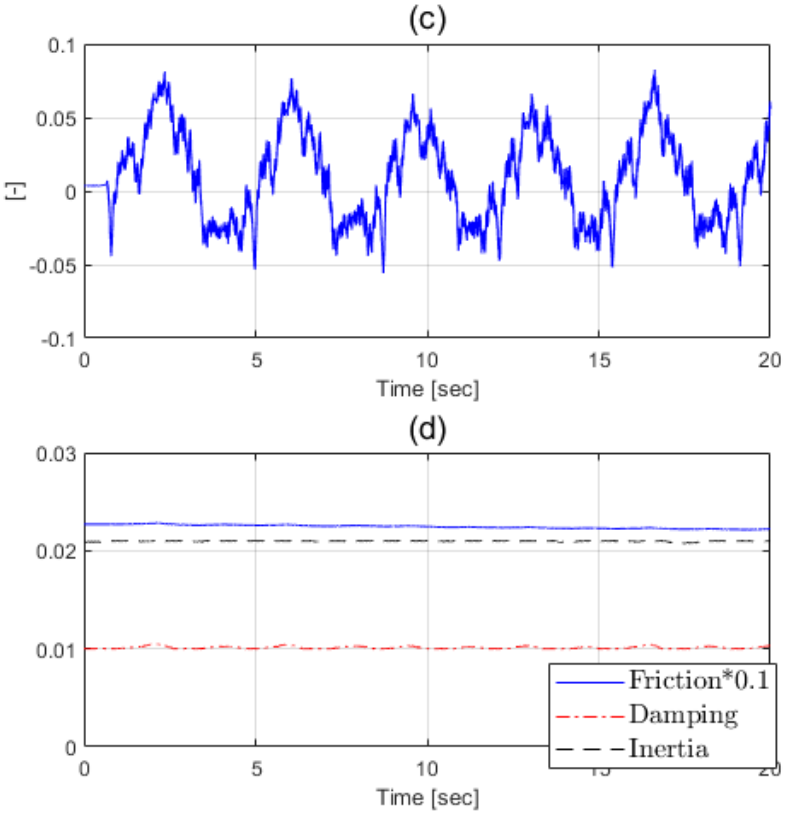

Figure 4.13 45deg weave test at 70km/h.

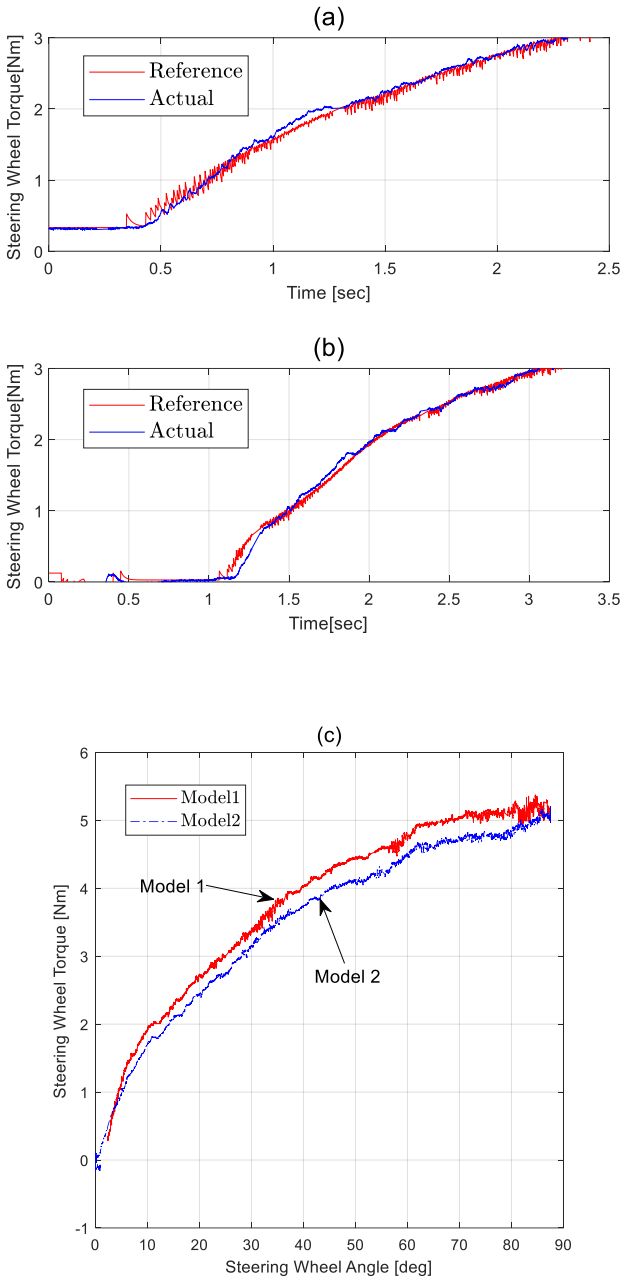

Figure 4.14 10 deg/s transition test at 70 km/h

To evaluate the proposed algorithm, the objective parameters are listed in Table 4. In the weave test, the average error of the parameters of the computer simulation is approximately 1.2%, and the average error of the HILS is approximately 7.0%. The objective parameter is illustrated in Table 5. In the transition test, the average error of the parameters of the computer simulation is approximately 0.1% and the average error of the HILS is approximately 10.15%.

Table 4 Comparison of computer simulation and HILS results using objective parameters with the weave test.

	Unit	Computer simulation		HILS	
		Target	Actual	Target	Actual
On-center stiffness	Nm/deg	0.2123	0.2089	0.2088	0.1989
Steering friction	Nm	1.6756	1.6654	1.7324	1.6264
Angle hysteresis	deg	10.286	10.124	11.2324	9.8542

Table 5 Comparison of computer simulation and HILS results using objective parameters with the transition test.

		Unit	Computer simulation		HILS	
			Target	Actual	Target	Actual
Average steering friction	Model 1	Nm	0.73	0.72	0.32	0.32
	Model 2		0.48	0.48	0.076	0.11
Off-center stiffness	Model 1	Nm/deg	0.069	0.07	0.108	0.112
	Model 2		0.07	0.07	0.092	0.098

Chapter 5 Conclusion and Future works

This dissertation has proposed a target steering wheel torque algorithm for application to an electric-power-assisted steering system (EPS) and steer-by-wire system (SBW). The tracking algorithm for EPS and SBW has been developed to overcome a major challenge of the conventional method, which is time-consuming tuning to achieve the desired steering feel. A target steering wheel torque map defined from the steering wheel angle, steering angular velocity, and vehicle speed gives drivers the desired steering feel. In the case of EPS control algorithm, the target steering wheel torque was tracked with an ASMC using an integral augmented sliding surface. The equivalent moment of inertia damping coefficient and effective compliance were adopted to achieve robust tracking performance. In addition, impedance control for SBW control algorithm has been developed to enhance the tracking performance of target steering feel.

The effectiveness of the proposed automated driving algorithm has been evaluated via test-data based simulations and hardware-in-the-loops (HILS) tests. The tests are performed with weave and transition tests. Especially, in the case of EPS algorithm, effective compliance, K_{eff} , plays a role in compensating for the error between the nominal rack force and the actual rack force, as can be seen in the simulation results. In addition, it was confirmed that

the effective compliance was dominant compared to other factors, as can be seen above from the results of experiments. The proposed EPS and SBW control algorithm achieved satisfactory steering wheel torque tracking performance.

Our future plans for the haptic control of steer-by-wire systems can be summarized into two major aspects. The first is to modify the target steering model. In this paper, the conventional motor-driven steering system has been targeted, but it does not provide the best steering feel. A study of the target steering model is important to improve the steering feel. The second plan concerns haptic control strategy in autonomous mode, in which a movement of the steering wheel can cause the driver to feel uncomfortable, so study of the quiet steering wheel should be conducted. Also, we will conduct the frequency domain analysis of the proposed controller. The adaptive sliding mode controller has a well- known trade-off problem, which occurs high-frequency oscillations by large adaptation gain, caused by adaptation gain tuning process.

Bibliography

Ahmadkhanlou, F., Washington, G. N., Bechtel, S. E., & Wang, Y. (2006). Magnetorheological fluid based automotive steer-by-wire systems. *Smart Structures and Materials 2006: Industrial and Commercial Applications of Smart Structures Technologies, 6171*.

Balachandran, A., & Gerdes, J. (2015). Designing Steering Feel for Steer-byWire Vehicles Using Objective Measures. *IEEE/ASME Transactions on Mechatronics, 20*(1), 373-383.

Bertollini, P., G., & Hogan, R. M. (1999.). Applying driving simulation to quantify steering effort preference as a function of vehicle speed. *SAE Technical Paper*, *1999-01-0394.*

Bevly, D. M., Ryu, J., & Gerdes, J. C. (2006). Integrating INS sensors with GPS measurements for continuous estimation of vehicle sideslip, roll, and tire cornering stiffness. *IEEE Transactions on Intelligent Transportation Systems 7.4*, 483-493.

Bidwell, B., J., & Cataldo., R. S. (1962, Feb. 27). *U.S. Patent No. 3,022,850.*

Chang, W.-D., & Yan., J.-J. (2005). Adaptive robust PID controller design based on a sliding mode for uncertain chaotic systems. *Chaos, Solitons & Fractals 26.1*, 167-175.

Chen, B. C., & Hsieh, F. C. (353-364). Sideslip angle estimation using extended Kalman filter. *Vehicle System Dynamics, 46(S1)*, 2008.

Cheon, D., & Nam, K. (2017). Steering torque control using variable impedance models for a steer-by-wire system. *International Journal of Automotive Technology 18(2)*, 263-270.

DeCarlo, R. A., Zak, S. H., & Matthews, G. P. (1988). Variable structure control of nonlinear multivariable systems: a tutorial. *Proceedings of the IEEE 76.3*, 212-232.

Eckstein, Hesse, L., Lutz, & Klein, M. (2014). Steer-by-Wire, Potential, and Challenges. *Encyclopedia of Automotive Engineering*, (pp. 1-14).

EkerI. (2006). Sliding mode control with PID sliding surface and experimental application to an electromechanical plant. "ISA transactions 45.1", 109-118.

Fankem, S., & Muller, S. (2014). A new model to computer the desired steering torque for steer-by-wire vehicles and driving simulators. *Vehicle System Dynamics, 52*, 251-271.

Farrer, & G, D. (1993). An objective measurement technique for the quantification of on-centre handling quality. *SAE Technical Paper*, *930827.*

Forsyth, B. A., & Maclean, K. E. (2006). Predictive haptic guidance: Intelligent user assistance for the control of dynamic tasks. *IEEE Trans. Vis. Comput. Graph., 12*(1), 103–113.

Gillespie, T. D. (1992). Fundamentals of vehicle dynamics. *SAE Technical Paper, 114*.

Green, P., Gillespie, T., Reifeis, S., L., W.-H., & Ottens, O. (1984). *Subjective evaluation of steering effort levels.* University of Michigan Transportation Research Intstitute UMYRI-84.

H., P., Sattavara, S., & Schechter, M. (1974, Aug 27). *U.S. Patent No. 3,831,701*.

Hayama, R., & Nishizaki, K. (2000). The vehicle stability Control Responsibility Improvement Using Steer-by-Wire. *Proceedings of the IEEE Intelligent Vehicles Symposium.*

Huang, Y. J., Kuo, T. C., & Chang, S. H. (2008). Adaptive sliding-mode control for nonlinear systems with uncertain parameters. *Systems, Man, and Cybernetics, Part B: Cybernetics, IEEE Transactions on 38.2*, 534-539.

Jang, B., Yi, K., Jung, C., Lee, J., Cha, Y. J., Park, J., & Park, J. (2014). Correlation of Subjective and Objective Measures of On-Center Handling. *SAE Technical Paper*, *2014-01-0128.*

Jiang, Y., Deng, W., Zhang, S., Wang, S., Zhao, Q., & Litkouhi, B. (2015). Studies on Influencing Factors of Driver Steering Torque Feedback. *AE Technical Paper*, *2015-01-1498.*

Keebler, & Jack. (1986). So long, hydraulics - the electronic revolution in power steering. *Popular Science. 228 (5)*, (pp. 50–56).

Kim, & Song. (2002). Control logic for an electric power steering system using assist motor. *Mechatronics 12.3*, (pp. 447-459).

Kim, C. J., Jang, J. H., Oh, S. K., Lee, J. Y., & Hedrick, J. K. (2008).

Development of a control algorithm for a rack-actuating steer-by-wire system using road information feedback. *Proceedings of the Institution of Mechanical Engineers Part D: Journal of Automobile Engineering, 222*(9), 1559–1571.

Koehn, Philip, & Eckrich., M. (2004). Active steering-the BMW approach towards modern steering technology. *SAE technical paper*, (pp. 2004-01-1105).

Kunnappillil Madhusudhanan, A., Corno, M., & Holweg, E. (2015). Sliding mode-based lateral vehicle dynamics control using tyre force measurements. *Vehicle System Dynamics*, 1-21.

Nakayama, T., & Suda, E. (1994). The present and future of electric power steering. *International Journal of Vehicle Design. 15: 243. Retrieved 8.*

Norman, & D, K. (1984). Objective evaluation of on-center handling performance. *SAE Technical Paper*, *840069.*

Nybacka, M., He, X., Su, Z., Drugge, L., & Bakker, E. (2014). Links between subjective assessments and objective metrics for steering, and evaluation of driver ratings. *Vehicle System Dynamics, 52.sup1*, 31-50.

Oh, S. W., Chae, H. C., Yun, S. C., & Han, C. S. (2004). The design of a controller for the steer-by-wire system. *JSME International Journal Series C 47.3*, (pp. 896-907).

Pacejka, H. B., & Besselink, I. J. (1997). Magic formula tyre model with transient properties. *Vehicle System Dynamics, 27(S1)*, 234-249.

Pfeffer, P. E., Harrer, M., & Johnston, D. N. (2008). Interaction of vehicle and steering system regarding on-centre handling. *Vehicle System Dynamics, 46(5)*, 413-428.

Piyabongkarn, D., Rajamani, R., Grogg, J. A., & Lew, J. Y. (2009). Development and experimental evaluation of a slip angle estimator for vehicle stability control. *IEEE Transactions on Control Systems Technology 17.1*, 78-88.

Setlur, P., Wagner, J. R., Dawson, D. M., & Braganza, D. (2006, Jan). A trajectory tracking steer-by-wire control system for ground vehicles. *IEEE Trans. Veh. Technol.*, *55*, pp. 76–85.

Slotine, E., J. J., & Li, W. (1991). *Applied nonlinear control* (Vol. 199). Englewood Cliffs: NJ: Prentice-hall.

Vadim, I. U. (1977). Survey paper variable structure systems with sliding modes. *IEEE Transactions on Automatic control 22.2.*

Wang, H., Kong, H., Man, Z. T., Cao, Z., & Shen, W. (2014). Sliding mode control for steer-by-wire systems with AC motors in road vehicles. *IEEE Trans. Ind. Electron.*, (pp. 1596–1611).

Yih, P., & Gerdes, J. C. (2005). Modification of vehicle handling characteristics via steer-by-wire. *Control Systems Technology, IEEE Transactions on 13.6*, 965-976.

Zhang, H., Zhang, Y., Liu, J., Ren, J., & Gao, Y. (2009). Modeling and characteristic curves of electric power steering system. *2009*

International Conference on Power Electronics and Drive Systems (PEDS), 1390-1393.

초 록

스티어 바이 와이어 조향감 재현을 위한 조향 반력 제어

본 논문은 종래의 조향 시스템 관점에서 전동식 동력 조향 (EPS) 시스템과 스티어 바이 와이어 (SBW) 조향 보조 토크 제어 알고리즘의 개발을 중점으로 하였습니다. 기존 조향 보조 토크 제어 알고리즘은 원하는 조향감을 구현하기 위해 종래의 시간 소모적 인 튜닝 방법을 사용합니다. 이러한 주요 단점을 극복하기 위해 새로운 조향 보조 제어 알고리즘을 개발하였습니다. 목표 스티어링 휠 토크 맵은 정현파(Weave test) 및 등속도 스티어링 입력 (Transition test) 모두에 대해 높은 등급의 조향감을 차량 테스트에서 얻은 후 데이터 처리를 하여 설계되었습니다. 스티어링 시스템의 불확실성에 대한 강건성을 보장하기 위해 적응 형 슬라이딩 모드 제어가 채택되었으며, 관성 모멘트 감쇠 계수와 컴플라이언스 계수(Effective compliance)가 제어기 성능을 개선하도록 적응형 파라미터로 선정되었습니다. 컴플라이언스 계수는 계산된 랙 힘과 실제 랙 힘 사이의 차이를 보상하는 역할을 했습니다. SBW

시스템의 경우, 이전에 제안 된 EPS 지원 토크 알고리즘을 개선하고 향상시키기 위해 임피던스 모델을 사용하였으며 스티어링 피드백 시스템에 적용되었습니다. SBW 시스템의 주요 과제 중 하나는 사람과 스티어링 휠 시스템 상호 작용에 의해 안정적인 작동과 사람에게 적절한 스티어링 피드백 토크를 제공하는 방법입니다. 임피던스 제어는 임피던스 모델 (타겟 스티어링 휠 토크 맵)과 컨트롤러 (적응 슬라이딩 모드 제어)로 구성됩니다. 따라서, 상기 제안 된 목표 조향 토크 맵을 이용함으로써 스티어 바이 와이어에서 스티어링 피드백 토크를 절절히 적용 됨을 확인 하였습니다.

제안 된 컨트롤러의 성능은 다양한 조향 조건에서 컴퓨터 시뮬레이션 및 HILS (Hardware-in-the-loop) 시뮬레이션을 수행하여 평가되었습니다. 제안 된 EPS 및 SBW 제어 알고리즘을 통해 최적의 스티어링 휠 토크 추적 성능을 달성했습니다.

주요어 : 전동식 조향 시스템, 스티어 바이 와이어, 차량 새시 제어, 자율주행, 하드웨어 인 루프 시뮬레이션기법

학 번: 2014-21839